Finite element reduced order models for nonlinear vibrations of piezoelectric layered beams with applications to NEMS

A. Lazarus [a,b], O. Thomas [a], J.-F. Deü [a,*]

[a] Structural Mechanics and Coupled Systems Laboratory, Cnam, 2 rue Conté 75003 Paris, France
[b] Department of Mechanical Engineering, Massachusetts Institute of Technology, Cambridge, MA 02139, USA

ABSTRACT

This article presents a finite element reduced order model for the nonlinear vibrations of piezoelectric layered beams with application to NEMS. In this model, the geometrical nonlinearities are taken into account through a von Kármán nonlinear strain–displacement relationship. The originality of the finite element electromechanical formulation is that the system electrical state is fully described by only a couple of variables per piezoelectric patches, namely the electric charge contained in the electrodes and the voltage between the electrodes. Due to the geometrical nonlinearity, the piezoelectric actuation introduces an original parametric excitation term in the equilibrium equation. The reduced-order formulation of the discretized problem is obtained by expanding the mechanical displacement unknown vector onto the short-circuit eigenmode basis. A particular attention is paid to the computation of the unknown nonlinear stiffness coefficients of the reduced-order model. Due to the particular form of the von Kármán nonlinearities, these coefficients are computed exactly, once for a given geometry, by prescribing relevant nodal displacements in nonlinear static solutions settings. Finally, the low-order model is computed with an original purely harmonic-based continuation method. Our numerical tool is then validated by computing the nonlinear vibrations of a mechanically excited homogeneous beam supported at both ends referenced in the literature. The more difficult case of the nonlinear oscillations of a layered nanobridge piezoelectrically actuated is also studied. Interesting vibratory phenomena such as parametric amplification or patch length dependence of the frequency output response are highlighted in order to help in the design of these nanodevices.

© 2011 Elsevier B.V. All rights reserved.

1. Introduction

Nanoelectromechanical systems or NEMS are systems consisting of integrated electromechanical resonators of nanometer-scale dimensions [1]. Thanks to the outstanding mechanical properties of the resonant nanostructure, such as its quality factor, NEMS response can exceed the quality of electrical signal from purely electronic devices. Recently, they have been proposed for use in ultrasensitive mass sensor [2], ultra high frequency electronic filters [3], bit storage systems [4] and radio-frequency telecommunication devices [5]. As researchers orient towards frequencies reaching the GHz, one of the key issue in the optimization of NEMS becomes the scaling down and the electromechanical efficiency of the actuation and detection process. Comparing to the more conventionally employed electrostatic excitations [6] or even the more original self-oscillation of

nanowires in field emission [7,8], NEMS based on piezoelectric actuation appears to be particularly advantageous due to the linearity of forcing, their intrinsic integrability, high-efficiency and low power consumption [9]. While the experimental realization of such NEMS with high electromechanical coupling remains an actual challenge [10], the predictive simulations of the nonlinear oscillations of these piezoelectrically laminated, and generally prestressed, slender nanostructures is no less a mandatory step in the future production of these devices.

In the scope of NEMS applications, the present study proposes a predictive model for nonlinear vibrations of piezoelectric layered beams. The nonlinear steady-state response is simulated with an original finite element reduced order model in order to enable every beam geometrical configurations for a reasonable computational time. Starting from a nonlinear finite element formulation of the considered laminated piezoelectric beam, the discrete problem is expanded on its truncated linear modal basis resulting in a low-order model. Only the latter needs then to be solved to compute the periodic beam oscillations either by a classical time integration method or in our case, by an original purely harmonic-based continuation tool [11,12].

* Corresponding author.
  E-mail addresses: alazarus@mit.edu (A. Lazarus),
olivier.thomas@cnam.fr (O. Thomas), jean-francois.deu@cnam.fr (J.-F. Deü).

Since first investigations in micro- and nanoelectromechanical systems have been conducted by experimental physicists, most of the theoretical models associated with the nonlinear vibrations of the resonant nanostructures are still heuristic models [13,14]. These approaches, although very convenient for the identification of electromechanical parameters of the nanosystems, are useless when dealing with the design or optimization of the resonator as heuristic models are not predictive.

One possibility to predict the behavior of nonlinear vibrating systems is the use of analytical models [15,16]. The nonlinear forced vibration of plates or shallow shells has been investigated in [17,18] by expanding the displacements of the structure on the linear natural modes and solving the associated low-order analytical model with a perturbation method. The case of a piezoelectrically excited plate at the nanoscale has been treated in [19] where the analytical steady-state solution is computed thanks to an asymptotic numerical continuation method. The method of averaging is used in [6] for determining the nonlinear dynamics of nanomechanical beam resonators electrostatically excited. Numerous papers, based on similar analytical methods and dedicated to the modeling of nonlinear vibration of piezoelectric beams can be found in the literature. Nonlinear free and forced oscillations of piezoelectric clamped–clamped microresonators have been studied in [20] and in [21] when lying in an electrostatic environment. The influence of imperfections on the nonlinear vibratory behavior of doubly supported sandwich piezoelectric beam has been treated in [22,23]. Analytical models of piezoelectrically actuated microcantilevers may be found in [24–26]. All these methods, although predictive and often relevant suffer a critical drawback: solving analytically the nonlinear equilibrium equations is only reasonable when dealing with structures with simple geometries.

A solution to free ourselves from this awkward geometry dependence is the use of finite element methods. The computation of large oscillations of homogeneous structures by coupling a nonlinear finite element analysis with a direct time integration procedure [27,28] or a harmonic balance method [29,30] is relatively well known today. The finite element modeling of nonlinear vibrations of piezoelectric structures is less common but has been treated in [31] or [32]. However, the vibratory responses of beams at the nanoscale are characterized by possible highly anharmonic steady-state response and very long transient response due to their outstanding quality factors. Consequently, NEMS are typical applications where the use of classical nonlinear finite element method lead to non-reasonable computational time and reduced order models become naturally relevant. Many reduction techniques for nonlinear dynamics have been developed by the mechanical engineering community. A finite element based nonlinear modal reduction may be found in [33] for the nonlinear vibration of rotating beams and in [34] when coupled with a temporal continuation method. The well-known proper orthogonal decomposition techniques are developed in [35] for

random excitation and in [36] for the particular case of electrostatically actuated MEMS. The reduction on a classical linear modal basis by determining the nonlinear modal stiffness coefficients for an arbitrary finite element model is explained in [37,38] and in [39] for uncertain geometrically nonlinear structures with stochastic methods. Finally, the enrichment of the linear vibration modes with their modal derivatives is described in [40,41] and in [42] for the MEMS nonlinear dynamic analysis.

In this paper, we choose to reduce our nonlinear finite element model on a linear modal basis following the method presented in [38]. Several reasons can explain this choice. One advantage of this method is the physical meaning of the linear eigenmodes which lead to criteria to select important eigenmodes. Also, this natural basis seems to be the most relevant to use for non-experienced computational scientists such as experimental physicists. Numerically, one needs only to compute the reduced order model once for a given geometry, the latter being valid for different external loading. Finally, our work is not limited to the description of the reduction technique implementation and has also some real practical applications to discuss the method. We will see in this paper that, even when dealing with a relatively simple one-dimensional piezoelectric layered model, questions relative to the choice and truncature of eigenvectors, or to the meaning of the nonlinear modal stiffness coefficients, are definitively not obvious and deserve to be treated for future application of this method.

The present article is divided into five main parts. After the present introduction, Section 2 exposes the details of a nonlinear finite element discretization of a laminated elastic beam with piezoelectric patches. This finite element model originality results mainly from a von Kármán nonlinear strain–displacement relationship and some relevant electrical assumptions leading to only one couple of variables per piezoelectric patches [43]. The modal expansion of the general finite element formulation is explained in Section 3. Details of the computation of the nonlinear modal stiffness coefficients as well as description of the original purely frequential continuation procedure used to compute the reduced order model are given in this section. In the last sections, we apply the above method to two numerical examples. In Section 4, we compute the nonlinear vibration of a simply supported homogeneous beam with different numerical methods in order to validate our approach. In Section 5, we perform the numerical simulations of a piezoelectric layered nanobeams in real geometrical configurations. We compare the numerical results obtained with our reduced order model with a classical full nonlinear finite element model.

2. An elastic beam with piezoelectric patches

This section is devoted to the general formulation of the nonlinear governing equations of a laminated beam composed of elastic and piezoelectric layers (Fig. 1). In this one-dimensional
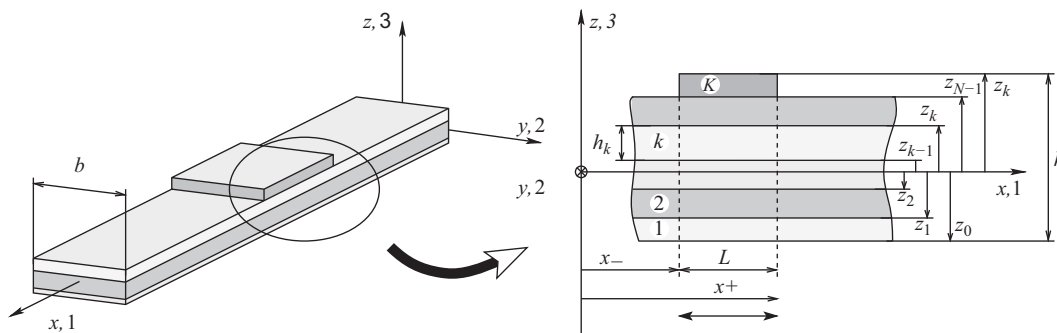

Fig. 1. Piezoelectric laminated beam.

model, we assume a von Kármán nonlinear strain–displacement relationships for taking into account the geometric nonlinearities associated with large amplitude oscillations of nanobeams. Using the finite element method with the electrical hypotheses of an elastic structure with piezoelectric patches described in [43], we are able to express the nonlinear variational formulation in terms of discrete variables such as the displacements at each nodes and the electrical potential of each patch.

2.1. Mechanical and electrical field assumptions

The beam is modeled using the classical laminate theory based on Euler–Bernoulli assumptions (Fig. 2 (left)). We limit our study to the vibration in the $(x-z)$ plane. The mechanical displacement field can then be written as

$$u_x(x,z,t) = u(x,t) + z\theta(x,t), \tag{1a}$$

$$u_z(x,z,t) = w(x,t), \tag{1b}$$

where u_x and u_z are the axial and transverse displacements; u is the axial displacement of the center line of the beam, w the transverse displacement, and θ the fiber rotation defined by

$$\theta = -\frac{\partial w}{\partial x}. \tag{2}$$

From the von Kármán nonlinear strain–displacement relationships and the above described kinematics, axial strain can be written as follows:

$$\varepsilon_1 = e + z\kappa, \tag{3}$$

where membrane strain e and curvature κ are defined by

$$e = \frac{\partial u}{\partial x} + \frac{1}{2}\left(\frac{\partial w}{\partial x}\right)^2 \quad \text{and} \quad \kappa = -\frac{\partial^2 w}{\partial x^2}. \tag{4}$$

Concerning the electrostatic aspects, we consider that the piezoelectric beams under study satisfy all assumptions expounded in [43]. In particular, the electric field vector, of components E_k, is normal to the electrodes and its magnitude is uniform in the piezoelectric patch p, so that for all $p \in \{1, \ldots, P\}$, the only non-vanishing component of the electric field is

$$E_3^{(p)} = -\frac{V^{(p)}}{h^{(p)}} n_3, \tag{5}$$

where $V^{(p)}$ is the potential difference of the p-th patch and n_3 is the component of the normal unit vector to the surface of the electrodes (see Fig. 1). In this case, two main coupling can be obtained: a "33" coupling between the transverse electric field and the stress/strain components in the same direction and a "31" coupling between the transverse electric field and the membrane stresses/strains (see Fig. 2 (right)). We recall from [43] that the present hypothesis is valid as long as the piezoelectric patches are thin, with a constant thickness, denoted $h^{(p)}$ for the p-th patch, smaller than its characteristic longitudinal length. Note that the piezoelectric patch

materials are transverse isotropic and the electric end effects for the piezoelectric patches are neglected.

2.2. Piezoelectric constitutive equations

Following the hypotheses of [43], the piezoelectric layers of the laminated beam are poled in the thickness $(z,3)$-direction with an electrical field applied parallel to this polarization. As said above, such a configuration is characterized in particular by the electromechanical coupling between the axial strain ε_1 and the transverse electrical field E_3. For sake of simplicity, we assume the classical plane-stress assumptions of beam theories ($\sigma_2 = \sigma_3 = 0$). The classical linear piezoelectric constitutive equations are restricted to the mechanical axial components only and reads:

$$\begin{cases} \sigma_1^k = Y^k \varepsilon_1 - e_{31}^k E_3, \\ D_3^k = e_{31}^k \varepsilon_1 + \epsilon_{33}^k E_3, \end{cases} \tag{6}$$

where σ_1^k and D_3^k are the axial stress and the transverse electrical displacement within the k-th layer, Y^k is the k-th layer Young's modulus in the $(1,2)$ plane at constant electric field, e_{31}^k is the piezoelectric constant and ϵ_{33}^k is the dielectric permittivity at constant strain. Note that Eq. (6) is a simple electromechanical approximation for constitutive behavior of one-dimensional beams, nevertheless fully sufficient in the scope of this paper. A more accurate Euler–Bernoulli model of laminated piezoelectric beam can be found in [44] where the influence of one-dimensional distribution of mechanical stresses and strains is taken into account through corrected electromechanical constitutive equations.

2.3. Variational formulation

Considering a particular axial part of the laminated beam (of length $L = x^+ - x^-$ and with a total of K layers including P piezoelectric patches as in Fig. 2), the variational formulation associated with the local equilibrium equation of our electromechanical system is given in [43] and can be expressed in the following form:

$$\sum_{k=1}^{K} \int_{\Omega^k} \rho^k(\ddot{u}_x \delta u_x + \ddot{u}_z \delta u_z)\, d\Omega + \sum_{k=1}^{K} \int_{\Omega^k} Y^k \varepsilon_1 \delta \varepsilon_1\, d\Omega$$

$$+ \sum_{p=1}^{P} \frac{V^{(p)}}{h^{(p)}} \int_{\Omega^{(p)}} e_{31}^{(p)} \delta \varepsilon_1\, d\Omega$$

$$= \sum_{k=1}^{K} \int_{\Gamma_t^k} (t_x^k \delta u_x + t_z^k \delta u_z)\, dS + \sum_{k=1}^{K} \int_{\Omega^k} (f_x^k \delta u_x + f_z^k \delta u_z)\, d\Omega, \tag{7a}$$

$$-\sum_{p=1}^{P} \frac{\delta V^{(p)}}{h^{(p)}} \int_{\Omega^{(p)}} e_{31}^{(p)} \varepsilon_1\, d\Omega + \sum_{p=1}^{P} V^{(p)} C^{(p)} \delta V^{(p)} = \sum_{p=1}^{P} Q^{(p)} \delta V^{(p)}, \tag{7b}$$

where ρ^k and Ω^k are the mass density and the domain occupied by the k-th layer and the p-th patch capacitance is

$$C^{(p)} = \frac{b l^{(p)}}{h^{(p)}} \epsilon_{33}^{(p)} \tag{8}$$

with b and $l^{(p)}$ are the width of the beam and the p-th patch length. Notice that the beam is subjected to surface axial and transversal forces at the boundaries of each face sublayer (t_x^k, t_z^k) and to body ones (f_x^k, f_z^k). The originality of the formulation is that the electrical state is fully described by only a couple of discrete variables per piezoelectric patches, namely the electric charge $Q^{(p)}$ contained in the electrode and the voltage $V^{(p)}$ between the electrodes. The electromechanical problem now consists in finding the admissible displacements u_i and the P electric charges $Q^{(p)}$ ($p \in \{1, \ldots, P\}$), such that the associated potential differences $V^{(p)}$
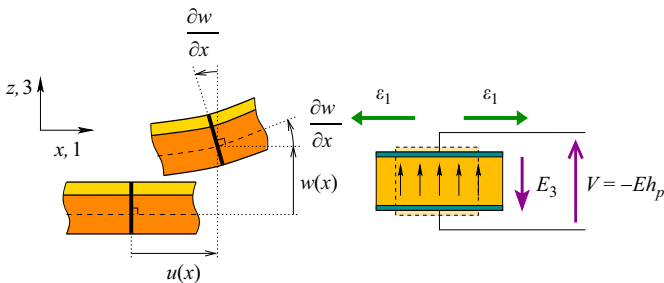

Fig. 2. Mechanical and electrical assumptions. (Left) Euler–Bernoulli hypothesis. (Right) "31" piezoelectric effect.

are prescribed, satisfying Eqs. (7a) and (7b) with appropriate initial conditions.

2.4. Finite element discretization

Using any finite element procedure to discretize the mechanical part of Eqs. (7a) and (7b) leads to introduce $\boldsymbol{u}$, the vector of nodal values of u_i. By introducing $Q^{(1)}Q^{(2)}\ldots Q^{(P)}$ and $V^{(1)}V^{(2)}\ldots V^{(P)}$, the electric charges and potential differences of the p-th patch, one finally obtains the general nonlinear finite element formulation of the laminated piezoelectric beam:

$$\boldsymbol{M}_m\ddot{\boldsymbol{u}}+\boldsymbol{K}_m\boldsymbol{u}+\boldsymbol{f}_{nl}(\boldsymbol{u})+\sum_{p=1}^{P}[\boldsymbol{f}_c^{(p)}+\boldsymbol{K}_c^{(p)}\boldsymbol{u}]V^{(p)}=\boldsymbol{f}_e,\tag{9a}$$

$$C^{(p)}V^{(p)}-Q^{(p)}-[\boldsymbol{f}_c^{(p)}+\boldsymbol{K}_c^{(p)}\boldsymbol{u}]^T\boldsymbol{u}=0\quad\forall p\in\{1\ldots P\}.\tag{9b}$$

In the above equation, $\boldsymbol{M}_m$ and $\boldsymbol{K}_m$ are the mechanical mass and stiffness matrices, of size $N\times N$, if N is the number of mechanical unknowns. Due to the assumed von Kármán strain–displacement relationships, the nonlinear part of the internal energy is represented by the N-dimensional column vector of nonlinear stiffness forces $\boldsymbol{f}_{nl}(\boldsymbol{u})$. $\boldsymbol{f}_e$ is the column vector of mechanical forcing, of length N. All details that lead to matrices $\boldsymbol{M}_m$, $\boldsymbol{K}_m$, $\boldsymbol{f}_{nl}(\boldsymbol{u})$ and $\boldsymbol{f}_e$ are written in Appendix A. $\boldsymbol{f}_c^{(p)}$ and $\boldsymbol{K}_c^{(p)}\boldsymbol{u}$ are the electromechanical coupling vectors, of size N, that couple the mechanical d.o.f. to the potential difference of the p-th patch only. In particular, $\boldsymbol{f}_c^{(p)}$ is the linear coupling vector found in the formulation of [43] and $\boldsymbol{K}_c^{(p)}$ is the $N\times N$ electromechanical matrix due to the nonlinear membrane/flexural coupling of the beam. Because of the von Kármán geometrical nonlinearities, a piezoelectric patch may induce some parametric excitations in the equilibrium equation (9a) through the vector $\boldsymbol{K}_c^{(p)}\boldsymbol{u}$. For an applied sinusoidal voltage $V^{(p)}$ with a frequency 2ω, the nanobeam is likely to oscillate with a fundamental frequency ω (see Section 5). Note that one single patch is generally discretized by more than one finite element such that $\boldsymbol{f}_c^{(p)}$ and $\boldsymbol{K}_c^{(p)}$ are simply obtained by assembling the elementary vectors $\boldsymbol{f}_c^{e(p)}$ of size (6×1) and elementary matrices $\boldsymbol{K}_c^{e(p)}$ of size (6×6), whose explicit expressions are given in Appendix A.

3. Reduced order model

In this section, a reduced-order formulation of the discretized problem obtained in Section 2 is introduced, by expanding the mechanical displacement unknown vector onto the short-circuit eigenmode basis. The main motivation of choosing this particular basis is that, beyond the physical meaning of these entities, it can be computed with a classical elastic mechanical problem, once for a given configuration. The unknown nonlinear stiffness coefficients in modal space are found by solving a set of prescribed displacements problems. Finally, the well-defined low-order model is recast in a quadratic dimensionless form for computing the periodic oscillation of our electromechanical system with an original harmonic-based continuation method.

3.1. Short-circuit normal modes

The system short circuit normal modes are solutions of Eq. (9a) with $V^{(p)}=0$ for all p, $\boldsymbol{f}_e=\boldsymbol{0}$ and $\boldsymbol{f}_{nl}(\boldsymbol{u})=\boldsymbol{0}$. The natural frequencies ω_i and mode shapes $\boldsymbol{\Phi}_i$ (each $\boldsymbol{\Phi}_i$ is a column vectors of length N) are the N eigensolutions of the following problem:

$$\boldsymbol{K}_m\boldsymbol{\Phi}-\omega^2\boldsymbol{M}_m\boldsymbol{\Phi}=\boldsymbol{0},\tag{10}$$

which depend only on the mechanical properties of the system.

These modes verify the following orthogonality properties:

$$\forall(i,j),\quad\boldsymbol{\Phi}_i^T\boldsymbol{M}_m\boldsymbol{\Phi}_j=\delta_{ij},\quad\boldsymbol{\Phi}_i^T\boldsymbol{K}_m\boldsymbol{\Phi}_j=\omega_i^2\delta_{ij},\tag{11}$$

where δ_{ij} is the Kronecker delta and the $\boldsymbol{\Phi}_i$ ($i=1,\ldots,N$) have been normalized with respect to the mass matrix:

$$\forall i,\quad\boldsymbol{\Phi}_i^T\boldsymbol{M}_m\boldsymbol{\Phi}_i=1.\tag{12}$$

One can note that the above equation imposes that the mode shapes $\boldsymbol{\Phi}_i$ units are $\text{kg}^{-1/2}$ for the elements linked to d.o.f. u and w and $\text{kg}^{-1/2}\,\text{m}^{-1}$ for the elements linked to d.o.f. θ (see Eq. (A.4) for the units of $\boldsymbol{M}_m$).

3.2. Modal expansion of the general problem

The displacement vector is sought as

$$\boldsymbol{u}(t)=\sum_{i=1}^{N}\boldsymbol{\Phi}_iq_i(t).\tag{13}$$

By inserting the above equation in Eqs. (9a) and (9b), multiplying the first obtained equation by $\boldsymbol{\Phi}_i^T$ and using the orthogonality properties of Eqs. (11), the problem writes, for all $i\in\{1,\ldots,N\}$:

$$\ddot{q}_i+2\xi_i\dot{q}_i+\omega_i^2q_i+\sum_{j=1}^{N}\sum_{k\geq j}^{N}\beta_{jk}^iq_jq_k+\sum_{j=1}^{N}\sum_{k\geq j}^{N}\sum_{l\geq j}^{N}\gamma_{jkl}^iq_jq_kq_l$$

$$+\sum_{p=1}^{P}\chi_i^{(p)}V^{(p)}+\sum_{p=1}^{P}\sum_{j=1}^{N}\Theta_{ij}^{(p)}q_jV^{(p)}=F_i,\tag{14a}$$

$$C^{(p)}V^{(p)}-Q^{(p)}-\sum_{j=1}^{N}\chi_j^{(p)}q_j-\sum_{j=1}^{N}\sum_{k=1}^{N}\Theta_{jk}^{(p)}q_jq_k=0.\tag{14b}$$

In Eq. (14a), $\chi_i^{(p)}$ is the linear electromechanical coupling coefficient of the i-th mode and the p-th piezoelectric patch, that is defined by

$$\chi_i^{(p)}=\boldsymbol{\Phi}_i^T\boldsymbol{f}_c^{(p)}\quad\forall i\in\{1\ldots N\},\ \forall p\in\{1\ldots P\}\tag{15}$$

and $\Theta_{ij}^{(p)}$ is the nonlinear electromechanical coefficient introducing the parametric excitation of the i-th mode, that is defined by

$$\Theta_{ij}^{(p)}=\boldsymbol{\Phi}_i^T\boldsymbol{K}_c^{(p)}\boldsymbol{\Phi}_j,\quad\forall i,j\in\{1\ldots N\},\ \forall p\in\{1\ldots P\}.\tag{16}$$

ξ_i and $F_i=\boldsymbol{\Phi}_i^T\boldsymbol{f}_e$ are respectively the modal viscous damping and the modal external forcing of the i-th mode. The quadratic and cubic polynomial stiffnesses of Eq. (14a) result from the modal expansion of the nonlinear internal forces $\boldsymbol{\Phi}_i^T\boldsymbol{f}_{nl}(\boldsymbol{u})$. Assuming von Kármán geometrical nonlinearities, these nonlinear internal forces are at most cubic in $\boldsymbol{u}$ (see Eq. (A.16)) and the governing equation (14a) is therefore exact.

The initial finite element formulation introduced in Section 2 has been replaced by the modal formulation of Eq. (14), whose unknowns are the N modal coordinates q_i and the P voltage/charge pairs $(V^{(p)},Q^{(p)})$ associated to the P piezoelectric patches. The reduced order model is then obtained by truncated the modal equation (14) to a number of M modes where M is generally much smaller than N. Its major interest, and especially the choice of the short-circuit eigenmodes as the expansion basis, is that the above computations of the parameters necessitates only *a single* modal analysis of the *elastic* problem. This operation can thus be done by any standard finite-elements code. To summarize, in order to obtain the finite element reduced order model of a given laminated piezoelectric beam, one has to:

- Compute all matrices and vectors of the initial problem (9), that is to say $\boldsymbol{M}_m$, $\boldsymbol{K}_m$, $\boldsymbol{f}_c^{(p)}$ and $\boldsymbol{K}_c^{(p)}$.
- Calculate the M natural frequencies ω_i under interest in short circuit as well as the associated mode shapes $\boldsymbol{\Phi}_i$, by solving the classical eigenvalues problem (10).

- Apply the matrix products (15) and (16) to obtain $\chi_i^{(p)}$ and $\Theta_{ij}^{(p)}$.
- Determine the unknown nonlinear stiffness coefficients β_{jk}^i and γ_{jkl}^i thanks to the following method.

3.3. Computation of nonlinear coefficients

The nonlinear modal stiffness coefficients β_{jk}^i and γ_{jkl}^i are computed with the method explained in [38]. Assuming the von Kármán relationship (4), the nonlinear stiffness forces $\boldsymbol{f}_{nl}(\boldsymbol{u})$ written in Appendix A are at most cubic in $\boldsymbol{u}$ and (14) is consequently exact. The procedure is based on the restoration of nodal applied forces by relevant prescribing nodal displacements in nonlinear static solution settings.

To illustrate the technique, one can begin by prescribing the displacement fields $\boldsymbol{u} = \boldsymbol{\Phi}_1 a$ and $\boldsymbol{u} = -\boldsymbol{\Phi}_1 a$ where a is an arbitrary constant scalar. In the modal formulations (13) and (14), this is equivalent to impose respectively:

$$q_1 = a \quad \text{and} \quad q_i = 0 \;\; \forall i \neq 1, \quad \boldsymbol{\Phi}_1^T \boldsymbol{f}_{nl}(\boldsymbol{\Phi}_1 a) = \beta_{11}^1 a^2 + \gamma_{111}^1 a^3, \quad (17a)$$

$$q_1 = -a \quad \text{and} \quad q_i = 0 \;\; \forall i \neq 1, \quad \boldsymbol{\Phi}_1^T \boldsymbol{f}_{nl}(-\boldsymbol{\Phi}_1 a) = \beta_{11}^1 a^2 - \gamma_{111}^1 a^3. \quad (17b)$$

The expanded nonlinear stiffness forces $\boldsymbol{\Phi}_1^T \boldsymbol{f}_{nl}(\boldsymbol{\Phi}_1 a)$ and $\boldsymbol{\Phi}_1^T \boldsymbol{f}_{nl}(-\boldsymbol{\Phi}_1 a)$ can be computed using (A.16) since a is a prescribed scalar and $\boldsymbol{\Phi}_1$ is known from the classical eigenvalues problem (10). From then, the coefficients β_{11}^1 and γ_{111}^1 can be determined from the resulting system (17) of two linear equations. Contrarily to [38], the relation (17) is exact in our case and theoretically independent on a. However, for numerical purposes, this constant scalar has to be consistent with the dimension of the finite element model to avoid bad conditioning. In the following, we simplify the computations and the explicit expressions by choosing $a=1$. By using an analogous manner to determine the coefficients β_{ii}^i and γ_{iii}^i for $i \neq 1$, one obtains the general formulae for the nonlinear stiffness coefficients with equal lower indices:

$$2\beta_{ii}^i = \boldsymbol{\Phi}_i^T(\boldsymbol{f}_{nl}(\boldsymbol{\Phi}_i) + \boldsymbol{f}_{nl}(-\boldsymbol{\Phi}_i)), \quad (18a)$$

$$2\gamma_{iii}^i = \boldsymbol{\Phi}_i^T(\boldsymbol{f}_{nl}(\boldsymbol{\Phi}_i) - \boldsymbol{f}_{nl}(-\boldsymbol{\Phi}_i)) \quad (18b)$$

$\forall i \in \{1 \ldots M\}$ where M is the number of retained eigenvectors. A similar technique can be employed to determine stiffness coefficients with two unequal lower indices. Prescribing the displacement fields in the form $\boldsymbol{u} = \pm \boldsymbol{\Phi}_j \pm \boldsymbol{\Phi}_k$ and summing the computed associated nonlinear stiffness forces $\boldsymbol{f}_{nl}(\boldsymbol{u})$, one obtains the relations:

$$2\beta_{jk}^i = \boldsymbol{\Phi}_i^T(\boldsymbol{f}_{nl}(\boldsymbol{\Phi}_j + \boldsymbol{\Phi}_k) + \boldsymbol{f}_{nl}(-\boldsymbol{\Phi}_j - \boldsymbol{\Phi}_k)) - 2\beta_{jj}^i - 2\beta_{kk}^i, \quad (19a)$$

$$2\gamma_{jjk}^i = -\boldsymbol{\Phi}_i^T(\boldsymbol{f}_{nl}(-\boldsymbol{\Phi}_j - \boldsymbol{\Phi}_k) + \boldsymbol{f}_{nl}(\boldsymbol{\Phi}_j - \boldsymbol{\Phi}_k)) + 2\beta_{jj}^i + 2\beta_{kk}^i - 2\gamma_{kkk}^i, \quad (19b)$$

$$2\gamma_{jkk}^i = \boldsymbol{\Phi}_i^T(\boldsymbol{f}_{nl}(\boldsymbol{\Phi}_j + \boldsymbol{\Phi}_k) + \boldsymbol{f}_{nl}(\boldsymbol{\Phi}_j - \boldsymbol{\Phi}_k)) - 2\beta_{jj}^i - 2\beta_{kk}^i - 2\gamma_{jjj}^i \quad (19c)$$

$\forall i,j,k \in \{1 \ldots M\}$ and $j < k$. Note that coefficients of this type appear only if $M \geq 2$. Finally, for cases where the number of retained eigenvectors is greater than or equal to three ($M \geq 3$), coefficients with three unequal lower indices may be determined by prescribing the displacement fields $\boldsymbol{u} = \boldsymbol{\Phi}_j + \boldsymbol{\Phi}_k + \boldsymbol{\Phi}_l$ and read

$$\gamma_{jkl}^i = \boldsymbol{\Phi}_i^T \boldsymbol{f}_{nl}(\boldsymbol{\Phi}_j + \boldsymbol{\Phi}_k + \boldsymbol{\Phi}_l) - \beta_{jj}^i - \beta_{kk}^i - \beta_{ll}^i - \beta_{jk}^i - \beta_{jl}^i - \beta_{kl}^i$$

$$-\gamma_{jjj}^i - \gamma_{kkk}^i - \gamma_{lll}^i - \gamma_{jjk}^i - \gamma_{jjl}^i - \gamma_{kkl}^i - \gamma_{jkk}^i - \gamma_{jll}^i - \gamma_{kll}^i \quad (20)$$

$\forall i,j,k,l \in \{1 \ldots M\}$ and $j < k < l$. With the nonlinear coefficients (18), (19) and (20), we have completely defined the upper triangular form of the nonlinear modal governing equations (14). Their

solutions can be undertaken through a large variety of techniques. In this paper, we will use an original purely frequential continuation procedure.

Remark. For practical purposes, an important number of coefficients β_{jk}^i and γ_{jkl}^i are equal to zero. For an obvious time computation issue, it is relevant to discard these negligible terms from the reduced order model. Numerically, a solution is to sort out the non-negligible terms by comparing the ratio between the coefficients and the average of the natural frequencies involved by the latters (the coefficient γ_{jkl}^i involves the natural frequencies ω_i, ω_j, ω_k and ω_l).

3.4. Continuation procedure

The nonlinear system of differential equations (14) is solved with the harmonic-based continuation software MANLAB [45]. This numerical tool, based on the classical harmonic balance method (HBM) and asymptotic numerical method (ANM), allowed us to continue the harmonic contributions of periodic solutions [11]. At each continuation step, the stability is assessed by computing and sorting the eigenvalues of the Hill matrix, which is simply the harmonic state operator of the computed periodic Jacobian of the dynamical system (14) as explained in [12].

Dealing with structures at the nanoscale and with first-order derivatives, the first mandatory step in the continuation procedure is to transform the finite element reduced order model (14) in a dimensionless form. We define L_0 as a characteristic length of the modeled structure and α_i as a scalar such that $\alpha_i = \max(\boldsymbol{\Phi}_i)$. Using $T_0 = 1/\omega_1$ as a characteristic time constant for the mechanical oscillator (14) and by normalizing the eigenvectors $\boldsymbol{\Phi}_i$ such that $\overline{\boldsymbol{\Phi}}_i = \alpha_i \boldsymbol{\Phi}_i$, we define the dimensionless variables

$$\bar{t} = \omega_1 t, \quad \overline{\boldsymbol{u}} = \frac{\boldsymbol{u}}{L_0}, \quad \overline{q}_i = \frac{q_i}{L_0 \alpha_i}, \quad \overline{\omega}_i = T_0 \omega_i, \quad \overline{F}_i = \frac{T_0^2}{L_0 \alpha_i} F_i,$$

$$\overline{\chi}_i^{(p)} = \frac{T_0^2}{L_0 \alpha_i} \chi_i^{(p)}, \quad \overline{\Theta}_{ij}^{(p)} = \frac{T_0^2 \alpha_j}{\alpha_i} \Theta_{ij}^{(p)},$$

$$\overline{\beta}_{jk}^i = T_0^2 L_0 \frac{\alpha_j \alpha_k}{\alpha_i} \beta_{jk}^i, \quad \overline{\gamma}_{jkl}^i = T_0^2 L_0^2 \frac{\alpha_j \alpha_k \alpha_l}{\alpha_i} \gamma_{jkl}^i. \quad (21)$$

At this stage, we do not consider the electrical equation (14b) which may be of interest if the patches are connected to an external electrical circuit. After simple calculations, the mechanical equilibrium (14a) may be rewritten in the first order dimensionless form of $2M$ equations (for a sake of clarity, variables written with our without bars will be considered dimensionless in the following):

$$\begin{cases} \dot{q}_i = p_i, \\ \dot{p}_i = -2\xi_i \omega_i p_i - \omega_i^2 q_i - \sum_{j=1}^M \sum_{k \geq j}^M \beta_{jk}^i q_j q_k - \sum_{j=1}^M \sum_{k \geq j}^M \sum_{l \geq k}^M \gamma_{jkl}^i q_j q_k q_l \\ \quad - \sum_{p=1}^P \chi_i^{(p)} V^{(p)} - \sum_{p=1}^P \sum_{j=1}^M \Theta_{ij}^{(p)} q_j V^{(p)} + F_i. \end{cases} \quad (22)$$

The leading idea of the harmonic-based continuation method used in [11,12] is to systematically recast the dynamical system (22) into a quadratic polynomial form. This procedure is fully explained in [11], which also shows that this quadratic recast can be applied to a large class of smooth systems with a few algebraic manipulations and a few additions of auxiliary variables. To illustrate the technique, we give an example of quadratic recast when the structure is excited by a mechanical harmonic forcing $\boldsymbol{f}_e(t) = \boldsymbol{f}_0 \cos(\omega t)$ (Section 4) and by several sinusoidal voltages $V^{(p)} = V_0^{(p)} \cos(\omega t)$ (Section 5). In that case, the new quadratic

system can be written as follows:

$$
\begin{cases}
\dot{q}_i = p_i, \\
\dot{p}_i = F_0^i \cos(\omega t) - 2\xi_i \omega_i p_i - \omega_i^2 q_i - \displaystyle\sum_{p=1}^{P} \chi_i^{(p)} V_0^{(p)} \cos(\omega t) \\
\quad - \displaystyle\sum_{p=1}^{P} \sum_{j=1}^{M} \Theta_{ij}^{(p)} q_j V_0^{(p)} X - \sum_{j=1}^{M} \sum_{k \geq j}^{M} \beta_{jk}^i q_j q_k - \sum_{j=1}^{M} \sum_{k \geq j}^{M} \sum_{l \geq k}^{M} \gamma_{jkl}^i q_j R_{kl}, \\
0 = R_{kl} - q_k q_l, \\
0 = \cos(\omega t) - X,
\end{cases} \quad (23)
$$

where the new unknown vector $\boldsymbol{z} = [q_1 \ldots q_L \ p_1 \ldots p_L \ R_{11} \ R_{12} \ldots R_{LL} \ X]^T$ contains the original components of the state vector $[q_1 \ldots q_L \ p_1 \ldots p_L]^T$ and some new variables added to get the quadratic form. A periodic solution of (23), of minimal period $T = 2\pi/\omega$, is expanded into the Fourier series

$$
\boldsymbol{z}_0(t) = \boldsymbol{z}_0 + \sum_{k=1}^{H} \boldsymbol{z}_c^k \cos(k\omega t) + \sum_{k=1}^{H} \boldsymbol{z}_s^k \sin(k\omega t) = \sum_{k=-H}^{H} \boldsymbol{z}_0^k e^{ik\omega t}. \quad (24)
$$

Using relation (24) in the governing equation (23) leads to an algebraic nonlinear system of $(2H+1) \times (2M+1+(M+M^2)/2)$ equations. From then, the ANM continuation method enables to compute the $\boldsymbol{z}_0^k$, $k = -H, \ldots, H$ for various contiguous values of control parameter $\lambda = \omega$, detect possible bifurcations and compute different branches of solutions. To assess the stability of these solutions, one needs to express the $2M \times 2M$ Jacobian of the dynamical system (22). To keep the computation efficiency of the continuation software [12], it is written in the quadratic form:

$$
\boldsymbol{J}(t) = \begin{bmatrix} \boldsymbol{0} & \boldsymbol{I} \\ -\boldsymbol{K}_0 & -\boldsymbol{C}_0 \end{bmatrix} + \begin{bmatrix} \boldsymbol{0} & \boldsymbol{0} \\ -\boldsymbol{K}_c(t) - \boldsymbol{K}_L(t) & \boldsymbol{0} \end{bmatrix} + \begin{bmatrix} \boldsymbol{0} & \boldsymbol{0} \\ -\boldsymbol{K}_Q(t) & \boldsymbol{0} \end{bmatrix}, \quad (25)
$$

where $\boldsymbol{K}_0$, $\boldsymbol{C}_0$, $\boldsymbol{K}_c(t)$, $\boldsymbol{K}_L(t)$ and $\boldsymbol{K}_Q(t)$ are expressed in Appendix B. In the above definitions, all matrices except $\boldsymbol{J}$ are of size $M \times M$, $\boldsymbol{0}$ being filled with zeros and $\boldsymbol{I}$ being the identity matrix. The quadratic first order dynamical system (23) and its Jacobian (25) are implemented in the MANLAB opensource software program [45]. MANLAB is an interactive software program for the continuation and bifurcation analysis of algebraic systems, based on ANM continuation. The latest version is programmed in Matlab using an object-oriented approach enhanced by fortran acceleration. It has a graphical user interface (GUI), with buttons, online inputs and graphical windows for generating, displaying and analyzing the bifurcation diagram and stability of the system. In the following, the nonlinear vibrations of two supported beams is treated by solving their finite element reduced order models with this software.
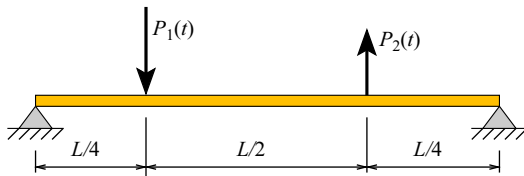
4. Test example: N.L. vibration of homogeneous beam

In this section, we validate the previous theoretical developments by computing the nonlinear oscillations of a simply supported homogeneous beam studied in [29,30]. This example being relatively simple, we are able to compare the results obtained with some classical analytical or finite element methods with our reduced order model.

4.1. System under study

The problem is to determine the nonlinear resonance curve for the simply supported beam subjected to external mechanical forces shown in Fig. 3 (left). The axial displacement is also prevented at each end. It is assumed a viscous damping matrix $\boldsymbol{D}_m$ proportional to the mass matrix so that $\boldsymbol{D}_m = c\boldsymbol{M}_m$ where $c/2\omega_1 = 0.005$ and ω_1 is the first natural frequency. The harmonic excitation forces read $P_1(t) = 13.63 EIr/l^3 \cos \lambda t$ and $P_2(t) = 9.62 EIr/l^3 \cos \lambda t$ where EI denotes the bending rigidity of the beam and $r = \sqrt{I/A}$ is the radius of gyration. The results, first computed in [29], are presented in Fig. 3 (right) where the modulus of non-dimensional amplitude of the first harmonic at $x = 0.75L$ versus the non-dimensional frequency λ/ω_1 is shown. In this work, the author computed the matrix amplitude equation of the discretized beam (eight elements) thanks to a Galerkin method. The resonance curve was obtained with an incremental-iterative continuation method and the stability was assessed with Floquet theory. Only the second and third harmonics were taken into account in the periodic solution but that was sufficient to qualitatively predict the internal resonance emerging from the system (visible in Fig. 3 (right) as the small slope).

We model the system of R. Lewandowsky with the method presented in Sections 2 and 3. In this purely mechanical problem, the electromechanical finite element formulation (9) reads simply:

$$
\boldsymbol{M}_m \ddot{\boldsymbol{u}} + \boldsymbol{D}_m \dot{\boldsymbol{u}} + \boldsymbol{K}_m \boldsymbol{u} + \boldsymbol{f}_{nl}(\boldsymbol{u}) = \boldsymbol{f}_e, \quad (26)
$$

where each matrix has been previously defined. In the following, we use a rectangular beam with a length $l = 1$ m, a width $b = 0.1$ m, a thickness $h = 0.001$ m, a Young modulus $E = 100$ MPa and a density $\rho = 2000$ kg/m^3.

4.2. Modal basis truncation

The eigenmodes of (26) are computed with the classical eigenvalue problem (10). Fig. 4 represents the first flexural modes $\boldsymbol{\Phi}_f$ and axial modes $\boldsymbol{\Phi}_a$ computed with Matlab for a simply supported beam discretized with 512 elements. The beam being homogeneous, the classical membrane and bending modes are totally decoupled.
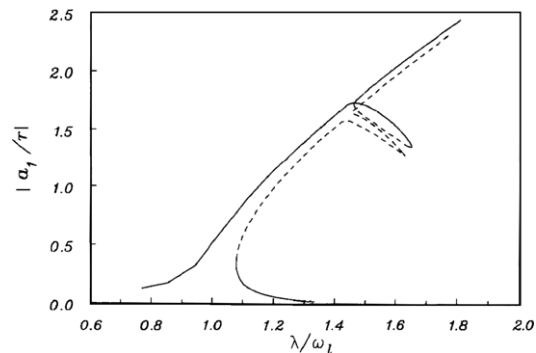

Fig. 3. Periodic vibration of geometrically nonlinear structures from R. Lewandowski [29]. (Left) Simply supported beam under the excitation forces. (Right) Resonance curve for $c/2\omega_1 = 0.005$.
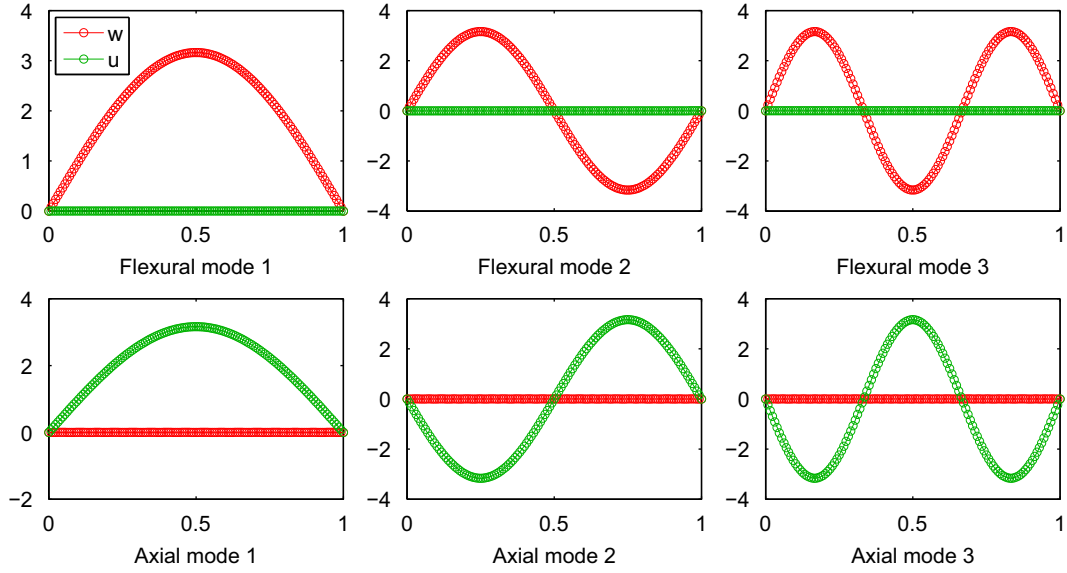
Fig. 4. Normal modes of the simply supported beam computed with 512 elements. First row: flexural modes. (Left) $\omega_{f1} = 3.21$ Hz. (Middle) $\omega_{f2} = 12.82$ Hz. (Right) $\omega_{f3} = 28.86$ Hz. Second row: axial modes. (Left) $\omega_{a1} = 3536$ Hz. (Middle) $\omega_{a2} = 7072$ Hz. (Right) $\omega_{a3} = 10\,609$ Hz.
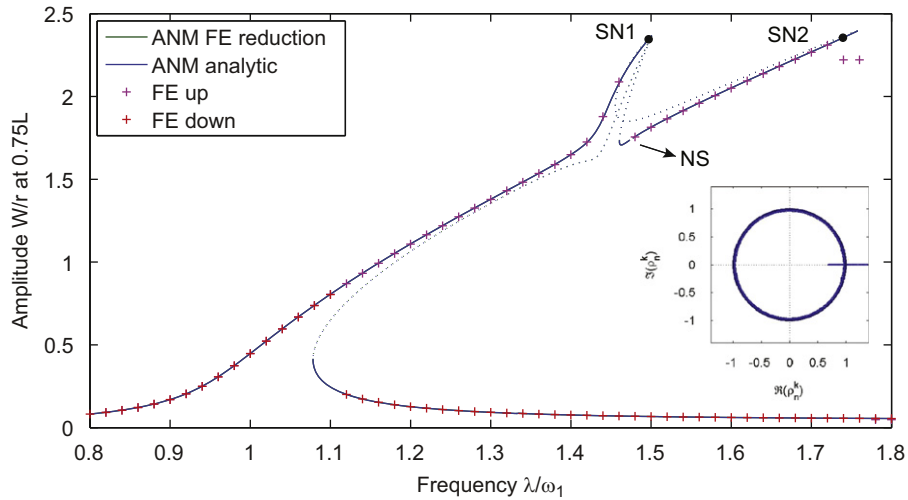

Fig. 5. Nonlinear frequency resonance around mode 1 obtained with different numerical method: ANM continuation of finite element reduced order model with three flexural modes, six axial modes and $H=10$, ANM continuation of classical analytical reduced order model with three modes and $H=10$ simulated harmonics, direct integration with 32 finite elements (Newmark average acceleration method + Newton–Raphson). Inset: Floquet multipliers of the perturbed solution represented in the unit circle. (For interpretation of the references to color in this figure legend, the reader is referred to the web version of this article.)

Expanding Eq. (26) on its modal basis $[\Phi_f \; \Phi_a]$ leads to the following purely mechanical reduced order model:

$$\ddot{q}_i + 2\xi_i \omega_i \dot{q}_i + \omega_i^2 q_i + \sum_{j=1}^{M}\sum_{k \geq j}^{M} \beta_{jk}^i q_j q_k + \sum_{j=1}^{M}\sum_{k \geq j}^{M}\sum_{l \geq k}^{M} \gamma_{jkl}^i q_j q_k q_l = F_i, \tag{27}$$

$\forall i,j,k,l \in \{1 \ldots M\}$ where M is the number of retained eigenvectors. All terms in Eq. (27) are computed according to Section 3 and $\xi_i = c/2\omega_i$.

4.3. Nonlinear vibratory behavior

Following the continuation procedure described in Section 3.4, we compute the harmonic contributions of each modal coordinates $q_i(t)$ of Eq. (27) from the quadratic dynamical system (23) with $V_0^{(p)} = 0 \; \forall p$. The stability of the periodic solution is determined through the quadratic Jacobian (25) with $V_0^{(p)} = 0 \; \forall p$ for each control parameter λ. The nonlinear oscillations of the beam are obtained by reconstructing the displacement vector with the modal recombination (13). The modulus of the maximal non-dimensional amplitude w/r of the beam oscillation at $x = 0.75L$ versus the non-dimensional excitation frequency λ/ω_1 is shown in Fig. 5 ($\omega_1 = \omega_{f1} = 3.21$ Hz is given in Fig. 4). The resonance curve and its stability have been obtained with the MANLAB continuation software when keeping the three first flexural modes and six first axial modes of the beam in the reduced order model. The number of simulated harmonics in the periodic solution is $H=10$. Stable solutions are plotted with full lines when unstable ones are characterized by dotted lines.

The resonance curve of Fig. 5 is in good agreement with the one obtained by R. Lewandowski, the qualitative differences

between Figs. 5 and 3 (right) being only due to the choice of plotted amplitudes. The stability regions of the saddle-node bifurcations are well predicted thanks to our original purely frequential stability analysis [12]. Besides the T-periodic instability regions of solutions with period $T = 2\pi/\lambda$ predicted by the Floquet multipliers (inset of Fig. 5), we detect a small quasiperiodic instability region leading to a Neimark–Sacker bifurcation near the internal resonance (point NS in Fig. 5). This instability is found with both analytical and finite element reduced order models and was not observed in [29]. The crosses in Fig. 5 are obtained with a direct integration of the complete finite element model with 32 elements by mixing a Newmark average acceleration algorithm and a Newton–Raphson method. The continuous full and dotted blue lines result from the continuation of an analytical reduced order model with 3 modes and 10 harmonics which similar formulations can be found in [19] for the nonlinear vibrations of a MEMS biosensor and in [16,46] for the nonlinear oscillations of a forced string. As visible, the results obtained by each method are very close. However, one has to keep in mind that the analytical model is only applicable because of the simple geometry of the studied structure and the direct finite element method do not compute every solutions of the problem (only the stable ones) since Eq. (26) is numerically integrated from the appropriately chosen initial condition up to time when the steady-state is reached. Moreover, the computation time of one steady-state solution using the direct finite element time integration method is greater than the time needed for the continuation

of our reduced order models. It is however difficult to emphasize the amount of time saved with our method in every cases since the necessary quadratic recast of Section 3.4 mixed with the harmonic balance method may significantly increase the number of equations to be solved and the MANLAB 1.0 continuation software used in this paper had some slowness due to the object-oriented approach in the Matlab language. In the future applications, the computation time should not be an issue anymore since the MANLAB 2.0 version enhanced computation using fortran acceleration [45].

Figs. 6 and 7 give an insight in the vibratory behavior of the beam at two critical points. The use of the short-circuit normal modes of Section 3.1 in our reduced order model is very relevant in our physical understanding of the problem. In particular, the bar chart of Fig. 6 shows that the SN1 point of the resonance curve displays a one-to-three internal resonance, i.e. a nonlinear coupling between the first harmonic of the first flexural mode and the third harmonic of the second flexural mode. Note that this complex nonlinear behavior could have been deduced from the linear analysis of Fig. 4 where $\omega_{f2} \approx 3\omega_{f1}$. The SN2 point of the resonance curve is simply the primary resonance of the first flexural mode as shown in Fig. 7. Another advantage of this numerical method is that the convergence, in terms of harmonics number and modal truncation, can be precisely checked. For 3 flexural modes, 6 axial modes and $H=10$ simulated harmonics, the solution is well converged since the bar graphs of Figs. 6 and 7 show that only the first harmonics of the two first flexural modes
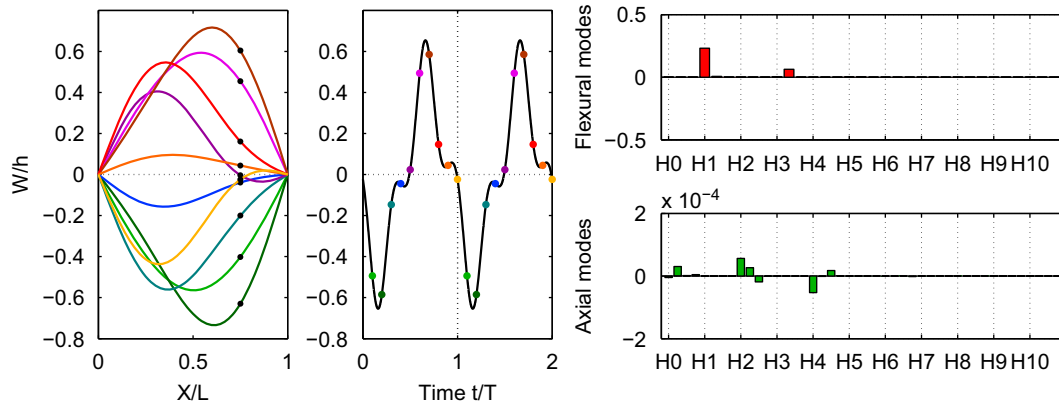

Fig. 6. Nonlinear vibratory response at the SN1 point of Fig. 5. (Left) Vibratory behavior of the supported beam. (Right) Amplitude of the harmonic contributions of the flexural and axial modes.
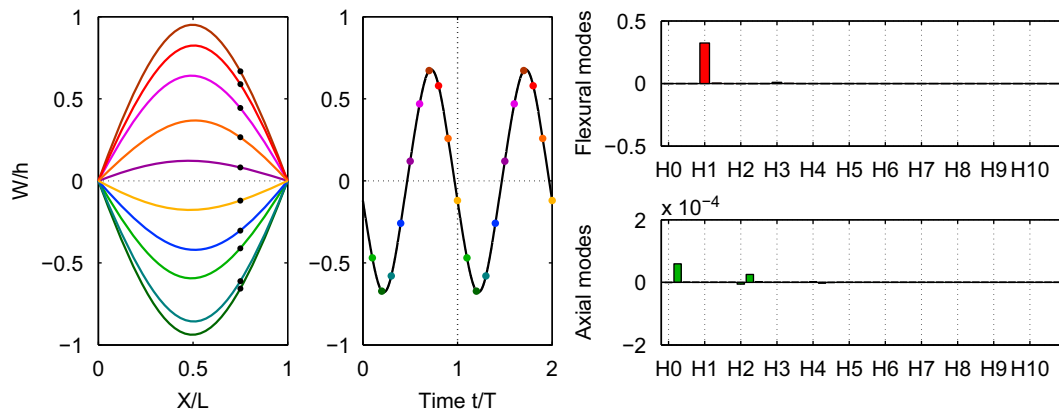

Fig. 7. Nonlinear vibratory response at the SN2 point of Fig. 5. (Left) Vibratory behavior of the supported beam. (Right) Amplitude of the harmonic contributions of the flexural and axial modes.

and the four first axial modes have a significant amplitude in the excitation frequency range. Note that both flexural modes and axial modes exist in the periodic oscillations at resonance.

4.4. Finite element and modal convergence

The finite element convergence is investigated in Fig. 8. As a classical result, the smaller is the considered computed natural frequency, the faster it converges to the exact analytical solution. An Euler–Bernoulli beam model with 10 elements is sufficient to approximate the sixth first natural frequencies at less than 1% from their exact values. Fig. 8 (right) shows the convergence of three nonlinear cubic coefficients γ_{jkl}^i towards their analytical counterparts. As in the frequency convergence, the higher is the mode involved in the coefficient calculation, the slower is the convergence. But in this case, we need much more finite elements to compute the nonlinear stiffness coefficients at less than 1% from their exact values. Moreover, the convergence is not smooth contrary to the one of Fig. 8 (left). The reason is that the computation of nonlinear coefficients is based on the restoration of nodal applied forces (see Section 3.3). The modeling accuracy of these internal nodal forces depends on the number of elements, and the same is true for the convergence. As a consequence, the convergence has a "sawtooth" shape where the period depends on the considered coefficient. The higher is the mode involved,

the larger is the period and the slower is the convergence. This awkward finite element dependence is not a real issue in our case since the computation of the coefficients is made only once and the number of retained eigenmodes is relatively small. However, this feature may explain the difficult convergence encountered when dealing with more complicated two-dimensional or three-dimensional structures such as in [38].

Fig. 9 shows the influence of modal truncation on the convergence of the resonance curve of the excited beam. As previously seen in Figs. 6 and 7, the axial modes are present in the periodic oscillation. Actually, one needs to retain some flexural modes in the solution to represent the vibratory behavior but it is also essential to keep sufficient axial modes to correctly model the flexural/membrane coupling of the system. The chosen method consists in retaining the first flexural modes and axial modes of the system up to the convergence. Fig. 9 (left) illustrates the location of the retained decoupled eigenmodes in the modal spectrum. In this simple test example, two flexural modes and four axial modes are sufficient to quantitatively compute the actual resonance curve of the beam (Fig. 9 (right)).

5. A piezoelectric layered nanobridge

The goal of this section is to predict the nonlinear oscillatory behavior of the piezoelectric layered nanobridges built by our
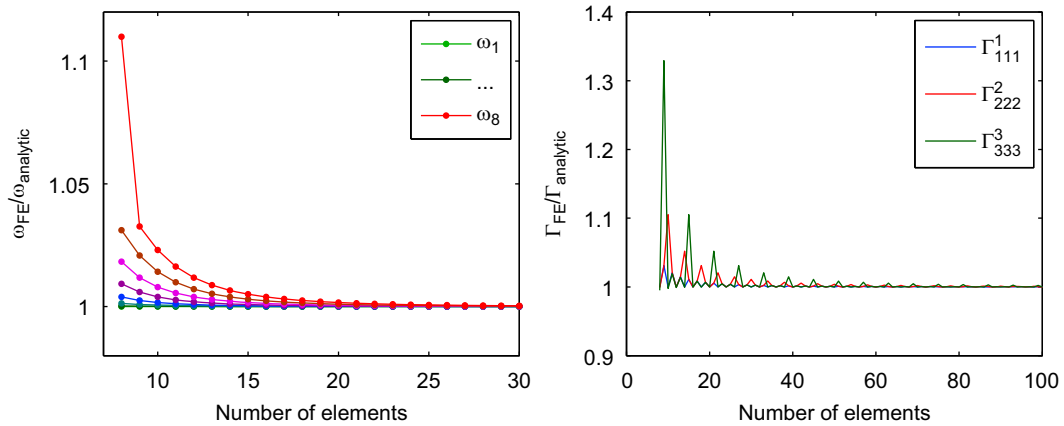

Fig. 8. Finite element convergence. (Left) On the natural frequencies. (Right) On the nonlinear modal stiffness cubic coefficients.
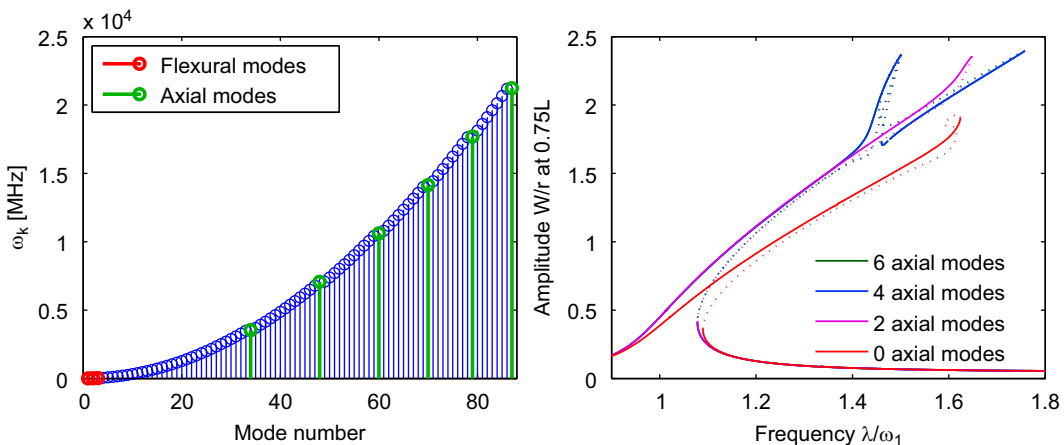

Fig. 9. Modal convergence. (Left) Localization of the retained eigenmodes in the modal spectrum. (Right) Influence of the number of axial modes on the computed resonance curves (with two flexural modes and $H=10$ simulated harmonics).
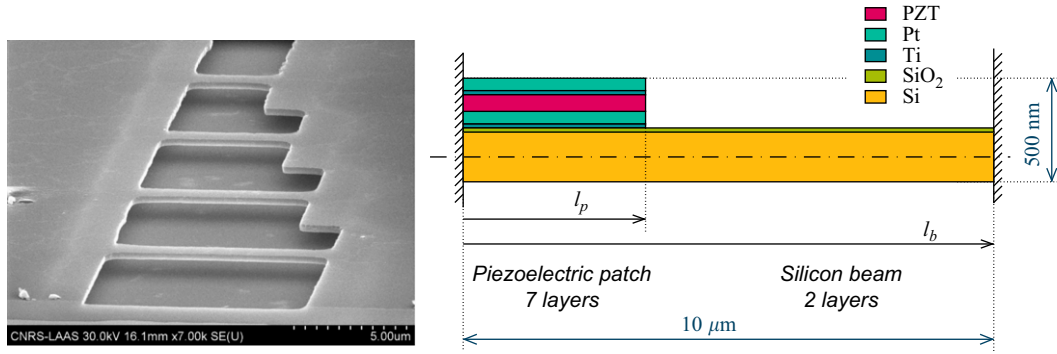
Fig. 10. A piezoelectric layered nanobeam. (Left) Scanning electron microscope image of several silicon nanobridges after liberation. Picture courtesy of LAAS, France. (Right) Sketch of the studied sample.

Table 1
Mechanical and geometrical properties of each layer of the nanobridge [48].

Material	Thickness (nm)	ρ (kg m^{-3})	E (GPa)	v
Si	340	2500	169	0.3
SiO$_2$	10	2150	70	0.17
Ti	10	4510	110	0.32
Pt	80	21 450	145	0.35
PZT	110	7800	96	0.45

physicist colleagues, from the LAAS laboratory in France, in order to help in the design of these upcoming devices. The beam is modeled with the finite element reduced order model explained in Sections 2 and 3 and validated in Section 4. The piezoelectric actuation of the slender layered structure lead to original and interesting vibratory phenomena dependent on the patch length.

5.1. System under study

The scanning electron microscope image of the devices under study is shown in Fig. 10 (left). The nanobridges are fabricated by employing stepper UV lithography on silicon on insulator (SOI) wafers [47]. From then, the technical challenge will be to deposit several activated electric layers at the nanoscale in order to piezoelectrically actuated the structure. For the numerical computations, we consider the slightly simplified sketch of the expected structures shown in Fig. 10 (right). Notably, the layers composing the piezoelectric patch have the same length and width and their thicknesses are constant along the patch. In that case, the patch is defined by only one parameter, its length l_p which is a fraction of the beam length l_b. We assume perfectly clamped boundary conditions and no slidings between each layer.

The mechanical and electrical properties of each layer is given in Table 1. The length of the beam is $l_b = 10$ μm but the patch length is not defined yet. Having no electrical external circuit connected to the patch and no mechanical external forces, the electromechanical finite element formulation of our model is simply

$$\boldsymbol{M}_m\ddot{\boldsymbol{u}} + \boldsymbol{K}_m\boldsymbol{u} + \boldsymbol{f}_{nl}(\boldsymbol{u}) + [\boldsymbol{f}_c + \boldsymbol{K}_c\boldsymbol{u}]V = \boldsymbol{0}, \tag{28}$$

where each matrix has been previously defined and with V prescribed.

5.2. Linear analysis

The eigenmodes of (28) are computed with the classical eigenvalue problem (10). Contrarily to the test example of Section 4, this eigenvalue problem is dependent on the patch length l_p. Fig. 11 shows the computed eigenfrequencies as

function of the patch length ratio l_p/l_b for a beam discretized with 512 elements. As visible, the influence of the patch geometry is important and some of the configurations may lead to nonlinear internal resonances if the frequency ratio ω_i/ω_1 is close to an integer value. This parametric linear analysis is a very convenient way to have a first insight in the intrinsic behavior of the design nanobridges.

Fig. 12 represents the first "flexural modes" $\boldsymbol{\Phi}_f$ and "axial modes" $\boldsymbol{\Phi}_a$ computed with Matlab for a laminated nanobridge with $l_p/l_b = 0.75$ discretized with 512 elements. Due to the presence of layers, the axial and transverse motions are linearly coupled and it is no more possible to refer to classical membrane and bending modes such as in Section 4. Since axial contribution is fundamental to model the flexural/membrane coupling of the nonlinear oscillations, we need to include some "axial modes" in the modal response. In this paper, we discriminate between the modes $\boldsymbol{\Phi}$ by comparing the integral of $u(x)$ and $w(x)$ along the length of the beam L. If the area below $w(x)$ is superior to the one below $u(x)$, the mode is a "flexural mode", otherwise, the mode is an "axial mode". Different visual methods have been tried to sort the $\boldsymbol{\Phi}_f$ and $\boldsymbol{\Phi}_a$ modes, though always based on the $u(x)$ and $w(x)$ contributions, but the present method was the most efficient. Expanding Eq. (28) on its modal basis $[\boldsymbol{\Phi}_f \ \boldsymbol{\Phi}_a]$ leads to the electromechanical reduced order model:

$$\ddot{q}_i + 2\xi_i\omega_i\dot{q}_i + \omega_i^2 q_i + \sum_{j=1}^{M}\sum_{k\geq j}^{M}\beta_{jk}^i q_j q_k + \sum_{j=1}^{M}\sum_{k\geq j}^{M}\sum_{l\geq j}^{M}\gamma_{jkl}^i q_j q_k q_l$$

$$+ \chi_i V + \sum_{j=1}^{M}\Theta_{ij}q_j V = 0, \tag{29}$$

$\forall i \in \{1 \ldots M\}$ where M is the number of retained eigenvectors and for one patch only. All terms in Eq. (29) are computed according to Section 3 and the modal damping ξ_i and applied voltage V are fixed in adequacy to the experimental expectations.

5.3. Nonlinear frequency response for $l_p/l_b = 3/4$

In order to avoid possible nonlinear internal resonances (see Fig. 11), we compute the nonlinear vibrations of a nanobridge with $l_p/l_b = 3/4$. We choose a modal damping $\xi_i = 0.01 \times \omega_1/\omega_i$ corresponding to a relatively small quality factor $Q = 1/2\xi = 50$, and a harmonic applied voltage $V = V_0 \cos(\Omega t)$ with $V_0 = 5$ V. The nonlinear coefficients are calculated with 512 elements. Following the continuation procedure described in Section 3.4, we compute the harmonic contributions of each modal coordinates $q_i(t)$ of Eq. (29) and their stability by using Eqs. (23) and (25) with $F_0^i = 0 \forall i$ (no mechanical external forces). For each control parameter Ω, the nonlinear oscillations of the nanobridge can
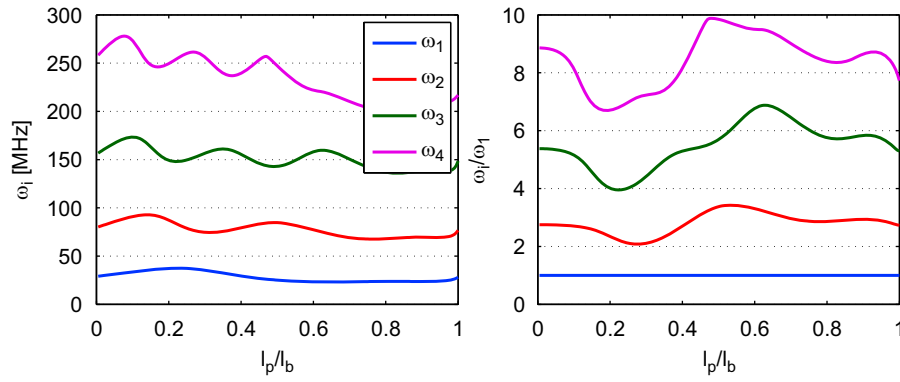
Fig. 11. Four first natural frequencies of the nanobridge as a function of patch length ratio l_p/l_b. (Left) Physical values. (Right) Dimensionless ratio ω_i/ω_1.
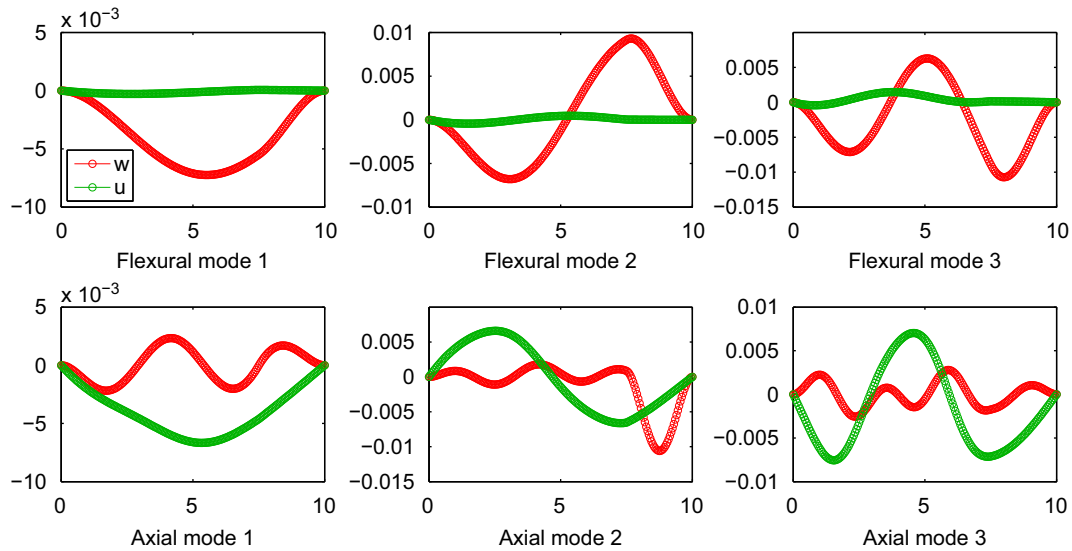

Fig. 12. Normal modes of the layered nanobridge with $l_p/l_b = 0.75$ (computed with 512 elements). First row: "flexural modes". (Left) $\omega_{f1} = 23.5$ MHz. (Middle) $\omega_{f2} = 67.7$ MHz. (Right) $\omega_{f3} = 142.1$ MHz. Second row: "axial modes". (Left) $\omega_{a1} = 203.7$ MHz. (Middle) $\omega_{a2} = 459.2$ MHz. (Right) $\omega_{a3} = 741.5$ MHz.
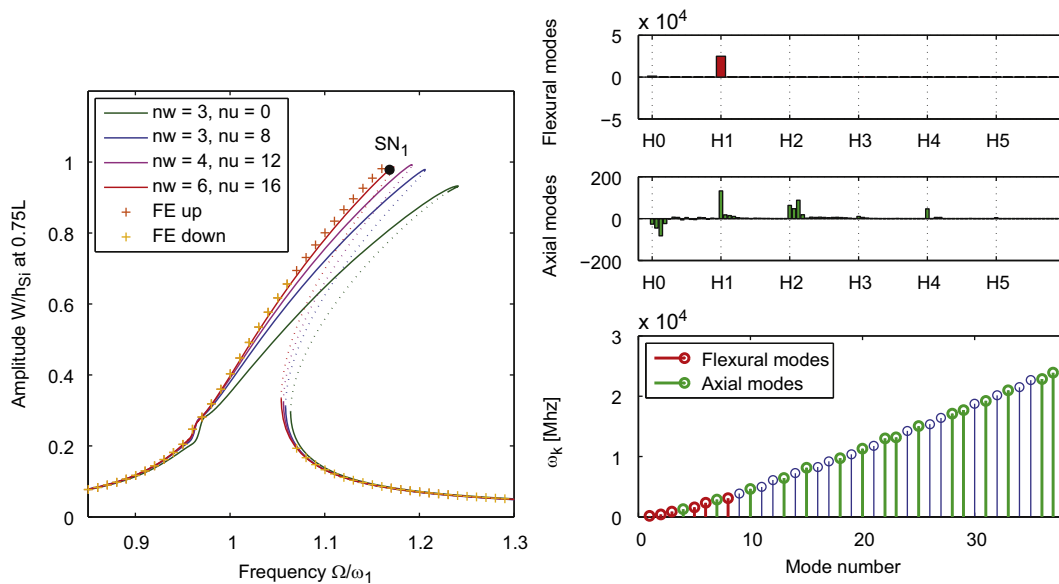
Fig. 13. Nonlinear frequency response around mode 1 at $x = 0.75l_b$ for $l_p/l_b = 3/4$. (Left) Influence of modal truncation on frequency response. (Right) Amplitude of the $H=5$ simulated harmonics with 6 "flexural modes" and 16 "axial modes" at the SN1 point of Fig. 13 (left). Localization of the retained eigenmodes in the modal spectrum.

be obtained by reconstructing the displacement vector with the modal recombination (13). The nonlinear frequency response around the first "flexural mode" is shown Fig. 13 when $H=5$ harmonics are retained in the solution. The modulus of the maximal non-dimensional amplitude (amplitude divided by the silicon thickness h_{Si}) of the beam oscillation at $x=0.75l_b$ versus the non-dimensional excitation frequency Ω/ω_1 ($\omega_1 = \omega_{f1} = 23.5$ MHz is given in Fig. 12) displays a classical resonance curve of hardening type whatever the number of retained "axial modes". However, one needs an important number of these "axial modes" to find a quantitative convergent solution with a correct stability region. For $n_w=6$ and $n_u=16$, the resonance curve is almost converged in terms of harmonics and tends to the steady-state response computed with the direct finite element time integration method used in the previous section (crosses in Fig. 13 (left)). In this highly layered case, the contribution of what we define as "axial modes" is not as efficient as in the homogeneous case and we need much more of these modes to harden the nonlinear resonance curve to the exact solution. Note that the maximum number of truncated modes was limited by the computational time of the first version of the MANLAB software.

The computed extended nonlinear frequency response of the piezoelectric layered beam is given Figs. 14 and 15. Notably, Fig. 14 represents the modulus of the maximal non-dimensional amplitude of the nanobridge oscillation at $x=0.75L$ versus the non-dimensional excitation frequency Ω/ω_1. An insight of the vibratory behavior at resonances is shown in Fig. 15. Due to the applied AC voltage, the system displays some nonlinear hardening resonances when the excitation frequency is close to the natural frequency of a "flexural mode". At the SN1 point, the beam vibrates mostly on its first mode with a fundamental frequency Ω (Fig. 15 (left)). At the SN3 point, the beam still oscillates with a period $2\pi/\Omega$ but mostly on its second flexural mode (Fig. 15 (right)). Note that these primary resonances are slightly nonlinear or anharmonic. Several small secondary resonances can be observed. The second "flexural mode" vibrates with a fundamental frequency 2Ω around $\Omega = 1.4\omega_1$ when the secondary resonance of the third "flexural mode" emerges around $\Omega = 3\omega_1$. Because of our chosen geometrical ratio l_p/l_b and the relatively small excitation amplitude, no internal resonances appear in the system.

As expected in Section 2, Fig. 14 shows that the T-periodic solution becomes unstable around $\Omega = 2\omega_1$ and bifurcates to a
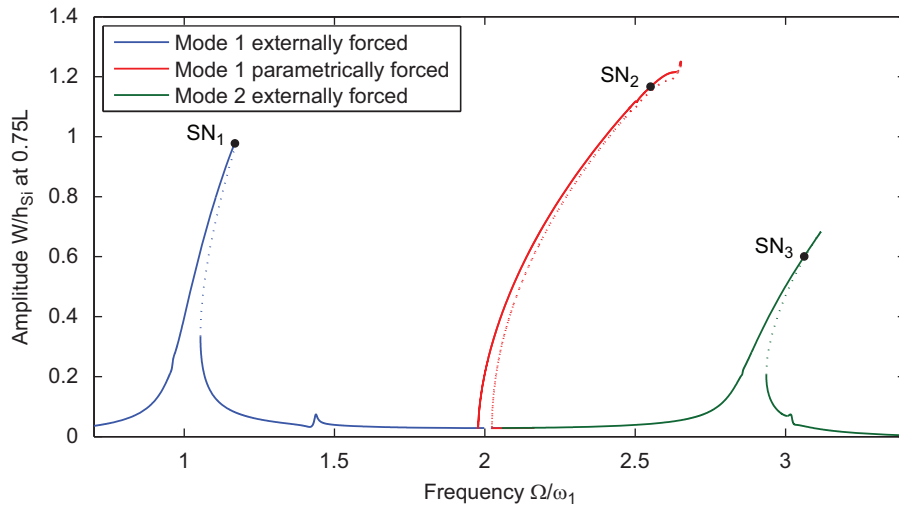

Fig. 14. Maximum amplitude of the vibratory response of the nanobridge with $l_p/l_b = 3/4$ at $x = 0.75l_b$ for 5 harmonics, 6 "flexural modes" and 16 "axial modes".
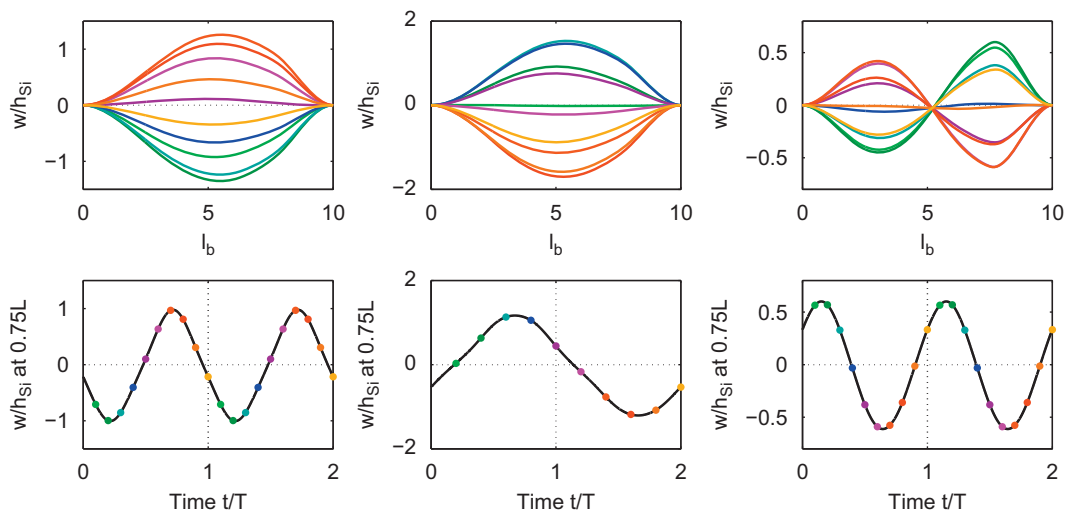

Fig. 15. Nonlinear vibratory response at resonances of Fig. 14. (Left) At point SN1. (Middle) At point SN2. (Right) At point SN3.
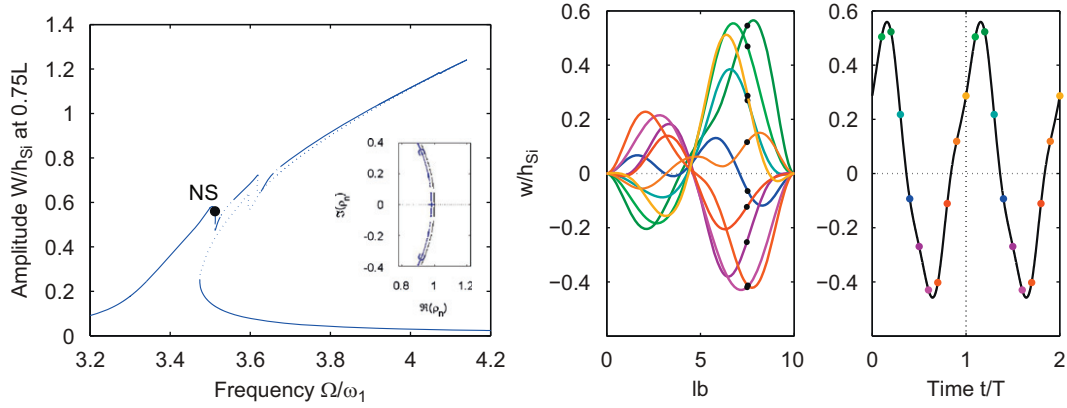
Fig. 16. Nonlinear vibratory response of the nanobridge with $l_p/l_b = 0.5$ for 6 harmonics, 5 "flexural modes" and 15 "axial modes". (Left) Maximum amplitude of the vibratory response at $x = 0.75l_b$. Inset: Floquet multipliers of the perturbed solution represented in the unit circle. (Right) Vibratory behavior at point NS.

2T-periodic solution. At the SN2 point, the structure vibrates mostly on its first "flexural mode" with a fundamental frequency $\Omega/2$, i.e. a period 2T, as shown in Fig. 15 (middle). Due to the parametric nature of the excitation, the amplitude of the 2T-periodic steady-state response exceeds the amplitude of the classic primary resonances. This original parametric feature has been experimentally investigated and exploited in [49]. Indeed, as the readout of mechanical motion becomes increasingly difficult as NEMS device are miniaturized, this parametric amplification (amplitude at SN2 point) can be useful to amplify the output signal in the mechanical domain. Finally, note that, the bifurcated 2T-periodic branch is numerically continued by adding the $\Omega/2$ harmonic contributions in the T-periodic solution. As a consequence, the computation time becomes longer and due to the continuation software limitations, this branch has been computed with eight harmonics, three "flexural modes" and eight "axial modes". This relatively small modal and frequential truncature may explained the curious behavior at the maximal value of the 2T-periodic branch.

5.4. Influence of patch length on the frequency response

Fig. 16 shows the nonlinear resonance curve of the doubled clamped piezoelectric beam with $l_p/l_b = 0.5$ for $H = 6$, $n_w = 5$ and $n_u = 15$. The modal damping is still $\xi_i = 0.01 \times \omega_1/\omega_i$ but we apply a harmonic voltage $V = V_0 \cos(\Omega t)$ with $V_0 = 2$ V. The system displays a two-to-four internal resonance, i.e. a nonlinear coupling between the first harmonic of the second "flexural mode" and the fourth harmonic of the fourth flexural mode. As a consequence, the beam vibrates mostly on its second flexural mode with a frequency $\Omega \approx \omega_{f2}$ but there is a non-negligible oscillation on the fourth flexural mode with a frequency $\omega_{f4} \approx 3\omega_{f2}$. Note that this complex nonlinear behavior could have been deduced from the linear analysis of Fig. 11 where $\omega_{f4} \approx 3\omega_{f2}$. Moreover, for some control parameter Ω, the Floquet multipliers tend to leave the unit circle with a non-zero imaginary part, predicting a Neimark–Sacker bifurcation of the steady-state solution. This means that during this resonance, a new frequency could appear in the solution. It is beyond the scope of this article to seek the new bifurcation branches and solutions. But this small example shows us an interesting mechanical behavior for the design of the upcoming devices. We may want to avoid these primary, parametric and internal resonances for the integrity of the structures but we may also make the most of these nonlinear phenomena. Indeed, these piezoelectric nanobridges behave as electronic high-frequency multipliers where the relation between the output and output signal is simply defined by the length of the patch. By playing with several patches, we should be able to realize even more difficult input–output operations.

6. Conclusions and discussions

An original finite element reduced order model for the nonlinear vibrations of piezoelectric layered beams has been presented. In this model, the geometrical nonlinearities are taken into account through a von Kármán nonlinear strain–displacement relationship. The originality of the finite element electromechanical formulation is that the system electrical state is fully described by only a couple of variables per piezoelectric patches, namely the electric charge contained in the electrodes and the voltage between the electrodes. Due to the geometrical nonlinearity, the piezoelectric actuation introduces an original parametric excitation term in the equilibrium equation. A reduced-order formulation of the discretized problem is obtained by expanding the mechanical displacement unknown vector onto the short-circuit eigenmode basis. Beyond its physical meaning, this basis is computed with the classical linear elastic mechanical problem, only once for a given geometrical configuration. A particular attention is paid to the computation of the unknown nonlinear stiffness coefficients of the reduced-order model. Due to the particular form of the von Kármán nonlinearities, these coefficients are computed exactly, once for a given geometry, by prescribing relevant nodal displacements in nonlinear static solutions settings. Finally, the previously defined low-order model is recast in a quadratic dimensionless form for computing the periodic oscillations (and theirs stability) of the electromechanical system with an original harmonic-based continuation method, particularly well-adapted for the analysis of NEMS generally characterized by very high quality factor. The presented method has been validated by computing the nonlinear vibrations of a mechanically excited homogeneous beam supported at both ends referenced in the literature. The more difficult case of the nonlinear oscillations of a layered nanobridge piezoelectrically actuated has also been studied. Interesting vibratory phenomena such as parametric amplification or patch length dependence of the frequency output response have been highlighted in order to help in the design of these nanodevices.

Although the presented self-sufficient method appears to be a very promising tool in the design of nonlinear oscillating beam structures such as piezoelectrically actuated NEMS, further investigations should be considered to improve the numerical method. Beyond the time computation inconveniences due to the employed continuation software version, it should be possible to accelerate the computation by discarding the negligible nonlinear modal stiffness coefficients. A simple method has been used for the moment but this is not sufficient and the term "negligible" needs to become clearer. This problem deserves a deeper

investigation to develop an efficient automatic numerical method of sorting. Another important theoretical issue remains the discrimination between the axial and flexural modes in the case of layered structures. More generally, a crucial question in the present reduction method is the choice of normal modes to include in the reduced order model. For our one-dimensional models, this modal convergence issue may be relegated to the background just by keeping an important number of modes in the solution. When extended the method to two-dimensional or three-dimensional structures where the coupling between axial and flexural modes is even more complicated, this modal truncature issue becomes a fundamental question. A future direction could be the use of modal derivatives or static modes, containing much beneficial reduction information, to enhance our solution.

Acknowledgments

Appendix A. Piezoelectric layered beam finite element discretization

Details of the layered beam finite element discretization of Section 2 are specified here, by starting from the variational formulation of Eqs. (7a) and (7b). In the following, a superscript or a subscript e refers to elementary quantities. The generalized displacements are discretized using linear (axial displacement) and cubic (transverse displacement) shape functions. Thus, axial and transverse displacements are related to the elementary d.o.f.'s vector $\boldsymbol{U}^e$ by

$$u^e = \boldsymbol{N}_u \boldsymbol{u}^e \quad \text{and} \quad w^e = \boldsymbol{N}_w \boldsymbol{u}^e, \tag{A.1}$$

where

$$\boldsymbol{u}^e = (u_1 \ w_1 \ \theta_1 \mid u_2 \ w_2 \ \theta_2)^T,$$

u_1, w_1 and θ_1 (respectively u_2, w_2 and θ_2) corresponding to the first (respectively second) node of the beam element.

In Eq. (A.1), the interpolation vectors are defined as follows:

$$\boldsymbol{N}_u = (N_1 \ 0 \ 0 \mid N_2 \ 0 \ 0)$$

and

$$\boldsymbol{N}_w = (0 \ N_3 \ N_4 \mid 0 \ N_5 \ N_6)$$

with, for all $x \in [0, L_e]$, where L_e is the elementary length,

$$N_1 = 1 - \frac{x}{L_e}, \quad N_2 = \frac{x}{L_e},$$

$$N_3 = \left(1 - \frac{x}{L_e}\right)^2 \left(1 + \frac{2x}{L_e}\right),$$

$$N_4 = x\left(1 - \frac{x}{L_e}\right)^2, \quad N_5 = \frac{x^2}{L_e^2}\left(3 - \frac{2x}{L_e}\right),$$

$$N_6 = \frac{x^2}{L_e}\left(\frac{x}{L_e} - 1\right).$$

Note that Eqs. (2), (4) and (A.1) lead to the following expression of elementary rotation, membrane strain and curvature

$$\theta^e = -\boldsymbol{N}_w' \boldsymbol{u}^e, \ e^e = \boldsymbol{N}_u' \boldsymbol{u}^e + \tfrac{1}{2}(\boldsymbol{N}_w' \boldsymbol{u}^e)^2 \quad \text{and} \quad \kappa^e = -\boldsymbol{N}_w'' \boldsymbol{u}^e, \tag{A.2}$$

where $(\cdot)' = \partial(\cdot)/\partial x = (\cdot)_{,x}$.

The various terms appearing in the variational formulation of Eqs. (7a) and (7b) are now successively discussed.

The kinetic energy variation is

$$\delta \mathcal{T} = \sum_{k=1}^N \int_{\Omega^k} \rho^k (\ddot{u}_x \delta u_x + \ddot{u}_z \delta u_z) \, d\Omega$$

$$= \int_{x^-}^{x^+} [I_0(\ddot{u}\delta u + \ddot{w}\delta w) + I_1(\ddot{u}\delta\theta + \ddot{\theta}\delta u) + I_2 \ddot{\theta}\delta\theta] \, dx$$

$$= \int_{x^-}^{x^+} (\delta u \ \delta w \ \delta \theta) \begin{pmatrix} I_0 & 0 & I_1 \\ 0 & I_0 & 0 \\ I_1 & 0 & I_2 \end{pmatrix} \begin{pmatrix} \ddot{u} \\ \ddot{w} \\ \ddot{\theta} \end{pmatrix} dx, \tag{A.3}$$

where the zero, first, and second order moments of inertia are defined by

$$[I_0, I_1, I_2] = \sum_{k=1}^N \rho^k [J_0^k J_1^k J_2^k],$$

with the zero, first and second moment of area of each sublayer respectively defined by

$$[J_0^k J_1^k J_2^k] = b^k \int_{z_{k-1}}^{z_k} [1, z, z^2] \, dz = b^k \left[h^k, \frac{z_k^2 - z_{k-1}^2}{2}, \frac{z_k^3 - z_{k-1}^3}{3} \right],$$

where b^k and h^k are the width and the thickness of the beam k-th layer. Applying the virtual work principle and assuming the discretized variation of kinetic energy is $\delta \mathcal{T}^e = \delta \boldsymbol{u}^{eT} \boldsymbol{M}_m^e \ddot{\boldsymbol{u}}^e$, the elementary mass matrix reads:

$$\boldsymbol{M}_m^e = \int_0^{L_e} (\boldsymbol{N}_u^T \ \boldsymbol{N}_w^T \ -\boldsymbol{N}_w'^T) \begin{pmatrix} I_0 & 0 & I_1 \\ 0 & I_0 & 0 \\ I_1 & 0 & I_2 \end{pmatrix} \begin{pmatrix} \boldsymbol{N}_u \\ \boldsymbol{N}_w \\ -\boldsymbol{N}_w' \end{pmatrix} dx,$$

whose explicit expression is

$$\boldsymbol{M}_m^e = \frac{I_0 L_e}{420} \begin{bmatrix} 140 & 0 & 0 & 70 & 0 & 0 \\ 0 & 156 & 22L_e & 0 & 54 & -13L_e \\ 0 & 22L_e & 4L_e^2 & 0 & 13L_e & -3L_e^2 \\ 70 & 0 & 0 & 140 & 0 & 0 \\ 0 & 54 & 13L_e & 0 & 156 & -22L_e \\ 0 & -13L_e & -3L_e^2 & 0 & -22L_e & 4L_e^2 \end{bmatrix}$$

$$+ \frac{I_1}{12} \begin{bmatrix} 0 & 6 & -L_e & 0 & -6 & L_e \\ 6 & 0 & 0 & 6 & 0 & 0 \\ -L_e & 0 & 0 & L_e & 0 & 0 \\ 0 & 6 & L_e & 0 & -6 & -L_e \\ -6 & 0 & 0 & -6 & 0 & 0 \\ L_e & 0 & 0 & -L_e & 0 & 0 \end{bmatrix}$$

$$+ \frac{I_2}{30L_e} \begin{bmatrix} 0 & 0 & 0 & 0 & 0 & 0 \\ 0 & 36 & 3L_e & 0 & -36 & 3L_e \\ 0 & 3L_e & 4L_e^2 & 0 & -3L_e & -L_e^2 \\ 0 & 0 & 0 & 0 & 0 & 0 \\ 0 & -36 & -3L_e & 0 & 36 & -3L_e \\ 0 & 3L_e & -L_e^2 & 0 & -3L_e & 4L_e^2 \end{bmatrix}. \tag{A.4}$$

The mechanical contribution to the internal energy variation is

$$\delta \mathcal{U} = \sum_{k=1}^N \int_{\Omega^k} Y^k \varepsilon_1 \delta\varepsilon_1 \, d\Omega = \int_{x^-}^{x^+} [Ae\delta e + B(\kappa\delta e + e\delta\kappa) + D\kappa\delta\kappa] \, dx$$

$$= \int_{x^-}^{x^+} (\delta e \ \delta \kappa) \begin{pmatrix} A & B \\ B & D \end{pmatrix} \begin{pmatrix} e \\ \kappa \end{pmatrix} dx, \tag{A.5}$$

where A is the extensional stiffness, D is the bending stiffness, and B is the bending–extensional coupling stiffness defined as

$$[A, B, D] = \sum_{k=1}^N Y^k [J_0^k J_1^k J_2^k].$$

Following Eq. (A.2), the discretized formulation of the variation of membrane strain and curvature is given by

$$\delta e^e = \mathbf{N}'_u \delta \mathbf{u}^e + \mathbf{N}'_w \mathbf{u}^e \mathbf{N}'_w \delta \mathbf{u}^e, \tag{A.6}$$

$$\delta \kappa^e = -\mathbf{N}''_w \delta \mathbf{u}^e. \tag{A.7}$$

Replacing δe, $\delta \kappa$, e and κ by their expressions and applying the virtual work principle to the weak form (A.5) leads to the discretized variation of the mechanical contribution to the internal energy variation

$$\delta \mathcal{U}^e = \delta \mathbf{u}^{eT} \mathbf{K}^e_m \mathbf{u}^e + \delta \mathbf{u}^{eT} \mathbf{f}^e_{nl}(\mathbf{u}^e), \tag{A.8}$$

where the elementary linear stiffness matrix reads

$$\mathbf{K}^e_m = \frac{A}{L_e}\begin{bmatrix} 1 & 0 & 0 & -1 & 0 & 0 \\ 0 & 0 & 0 & 0 & 0 & 0 \\ 0 & 0 & 0 & 0 & 0 & 0 \\ -1 & 0 & 0 & 1 & 0 & 0 \\ 0 & 0 & 0 & 0 & 0 & 0 \\ 0 & 0 & 0 & 0 & 0 & 0 \end{bmatrix} + \frac{B}{L_e}\begin{bmatrix} 0 & 0 & -1 & 0 & 0 & 1 \\ 0 & 0 & 0 & 0 & 0 & 0 \\ -1 & 0 & 0 & 1 & 0 & 0 \\ 0 & 0 & 1 & 0 & 0 & -1 \\ 0 & 0 & 0 & 0 & 0 & 0 \\ 1 & 0 & 0 & -1 & 0 & 0 \end{bmatrix}$$

$$+ \frac{D}{L_e^3}\begin{bmatrix} 0 & 0 & 0 & 0 & 0 & 0 \\ 0 & 12 & 6L_e & 0 & -12 & 6L_e \\ 0 & 6L_e & 4L_e^2 & 0 & -6L_e & 2L_e^2 \\ 0 & 0 & 0 & 0 & 0 & 0 \\ 0 & -12 & -6L_e & 0 & 12 & -6L_e \\ 0 & 6L_e & 2L_e^2 & 0 & -6L_e & 4L_e^2 \end{bmatrix} \tag{A.9}$$

and where the explicit expression of the nonlinear internal elementary forces $\mathbf{f}^e_{nl}(\mathbf{u}^e)$ is given at the end of this Appendix.

Work done by the external mechanical forces

$$\delta \mathcal{W} = \sum_{k=1}^{K} \int_{\Gamma^k_t} (t^k_x \delta u_x + t^k_z \delta u_z)\, dS + \sum_{k=1}^{K} \int_{\Omega^k} (f^k_x \delta u_x + f^k_z \delta u_z)\, d\Omega$$

$$= \sum_{k=1}^{K} \left\{ \left[\int_{\Sigma^k} (t^k_x \delta u + t^k_z \delta w - z t^k_x \delta \theta)\, dS \right]_{x^-}^{x^+} + \int_{\Omega^k} (f^k_x \delta u + f^k_z \delta w - z f^k_x \delta \theta)\, d\Omega \right\}$$

$$= [N\delta u + T\delta w - M\delta \theta]_{x^-}^{x^+} + \int_{x^-}^{x^+} (n\delta u + t\delta w - m\delta \theta)\, dx, \tag{A.10}$$

where Σ^k is the cross-section area of the layer k and where the boundary and distributed (i) normal resultant, (ii) shear resultant and (iii) bending moment are respectively defined by

$$[N,T,M] = \sum_{k=1}^{K} \left[\int_{\Sigma^k} t^k_x\, dS, \int_{\Sigma^k} t^k_z\, dS, \int_{\Sigma^k} z t^k_x\, dS \right]$$

and

$$[n,t,m] = \sum_{k=1}^{K} \left[\int_{\Sigma^k} f^k_x\, dS, \int_{\Sigma^k} f^k_z\, dS, \int_{\Sigma^k} z f^k_x\, dS \right].$$

The elementary vector of generalized mechanical forces is then

$$\mathbf{f}^e_e = [N\mathbf{N}^T_u + T\mathbf{N}^T_w + M\mathbf{N}'^T_w]^{L_e}_0 + \int_0^{L_e} (n\mathbf{N}^T_u + t\mathbf{N}^T_w + m\mathbf{N}'^T_w)\, dx,$$

whose explicit expression is

$$\mathbf{f}^e_e = \begin{bmatrix} N \\ T \\ M \\ 0 \\ 0 \\ 0 \end{bmatrix}_{x=0} + \begin{bmatrix} 0 \\ 0 \\ 0 \\ in \\ T \\ M \end{bmatrix}_{x=L_e} + \frac{nL_e}{2}\begin{bmatrix} 1 \\ 0 \\ 0 \\ 1 \\ 0 \\ 0 \end{bmatrix} + \frac{tL_e}{12}\begin{bmatrix} 0 \\ 6 \\ L_e \\ 0 \\ 6 \\ -L_e \end{bmatrix} + m\begin{bmatrix} 0 \\ -1 \\ 0 \\ 0 \\ 1 \\ 0 \end{bmatrix}. \tag{A.11}$$

The piezoelectric contributions of the internal energy variation, related to the inverse effect, is

$$\delta \mathcal{U}_c = \sum_{p=1}^{P} \frac{V^{(p)}}{h^{(p)}} \int_{\Omega^{(p)}} e^{(p)}_{31} \delta \varepsilon_1\, d\Omega = \sum_{p=1}^{P} \left[\int_{x^-}^{x^+} G^{(p)}_0 V^{(p)} \delta e\, dx + \int_{x^-}^{x^+} G^{(p)}_1 V^{(p)} \delta \kappa\, dx \right]$$

$$= \sum_{p=1}^{P} \int_{x^-}^{x^+} (\delta e\ \ \delta \kappa) \begin{pmatrix} G^{(p)}_0 \\ G^{(p)}_1 \end{pmatrix} V^{(p)}\, dx, \tag{A.12}$$

where $G^{(p)}_0$ and $G^{(p)}_1$ are defined by

$$[G^{(p)}_0, G^{(p)}_1] = \frac{e^{(p)}_{31}}{h^{(p)}} [J^{(p)}_0\ J^{(p)}_1].$$

Thanks to the virtual work principle, the discretized variation of the piezoelectric contributions to the internal energy variation can be written as

$$\delta \mathcal{U}^e_c = \delta \mathbf{u}^{eT} \mathbf{f}^{e(p)}_c + \delta \mathbf{u}^{eT} \mathbf{K}^{e(p)}_c \mathbf{u}^e \tag{A.13}$$

leading to the elementary coupling vector

$$\mathbf{f}^{e(p)}_c = \int_0^{L_e} (\mathbf{N}'^T_u\ \ -\mathbf{N}''^T_w) \begin{pmatrix} G^{(p)}_0 \\ G^{(p)}_1 \end{pmatrix} dx = G^{(p)}_0 \begin{bmatrix} -1 \\ 0 \\ 0 \\ 1 \\ 0 \\ 0 \end{bmatrix} + G^{(p)}_1 \begin{bmatrix} 0 \\ 0 \\ 1 \\ 0 \\ 0 \\ -1 \end{bmatrix} \tag{A.14}$$

and elementary coupling matrix

$$\mathbf{K}^{e(p)}_c = \int_0^{L_e} \mathbf{N}'^T_w G^{(p)}_0 \mathbf{N}'_w\, dx = \frac{G^{(p)}_0}{30L}\begin{bmatrix} 0 & 0 & 0 & 0 & 0 & 0 \\ 0 & 36 & 3L_e & 0 & -36 & 3L_e \\ 0 & 3L_e & 4L_e^2 & 0 & -3L_e & -L_e^2 \\ 0 & 0 & 0 & 0 & 0 & 0 \\ 0 & -36 & -3L_e & 0 & 36 & -3L_e \\ 0 & 3L_e & -L_e^2 & 0 & -3L_e & 4L_e^2 \end{bmatrix}. \tag{A.15}$$

The same vectors and matrices are obtained for the direct effect.

$$\mathbf{f}^e_{nl}(\mathbf{u}^e) = \frac{A}{L^3}\begin{bmatrix} \frac{L}{30}(-18w_1^2 - 3w_1\theta_1 L + 36w_1 w_2 - 3w_1\theta_2 L - 2\theta_1^2 L^2) \\ \frac{1}{280}(-864w_1^2 w_2 + 864 w_1 w_2^2 - 288w_2^3 + 288w_1^3 \\ -\theta_2^3 L^3 - \theta_1^3 L^3 - 216w_1 w_2\theta_2 L + 28L^2 u_2\theta_1 + 28L^2 u_2\theta_2) \\ \frac{L}{840}(18w_1\theta_1 L^2\theta_2 - 18\theta_1 L^2 w_2\theta_2 - 324w_1^2 w_2 + 324w_1 w_2^2 \\ -108w_2^3 + 108w_1^3 - 3\theta_2^3 L^3 + 24\theta_1^3 L^3) \\ \frac{L}{30}(18w_1^2 + 3w_1\theta_1 L - 36w_1 w_2 + 3w_1\theta_2 L + 2\theta_1^2 L^2) \\ \frac{1}{280}(864w_1^2 w_2 - 864w_1 w_2^2 + 288w_2^3 - 288w_1^3 + \theta_2^3 L^3 + \theta_1^3 L^3 \\ +216w_1 w_2\theta_2 L - 28L^2 u_2\theta_1 - 28L^2 u_2\theta_2) \\ \frac{L}{840}(18w_1\theta_1 L^2\theta_2 - 18\theta_1 L^2 w_2\theta_2 - 324w_1^2 w_2 + 324w_1 w_2^2 \\ -108w_2^3 + 108w_1^3 + 24\theta_2^3 L^3) \end{bmatrix}$$

$$+ \frac{A}{L^3}\begin{bmatrix} \frac{L}{30}(3\theta_1 L w_2 + \theta_1 L^2\theta_2 - 18w_2^2 + 3w_2\theta_2 L - 2\theta_2^2 L^2) \\ \frac{1}{280}(336Lu_2 w_1 - 336Lu_2 w_2 + 108w_2^2\theta_2 L - 36w_2\theta_2^2 L^2 \\ -28L^2 u_1\theta_1 + 108\theta_1 L w_2^2 + 3\theta_1 L^3\theta_2^2 - 216w_1\theta_1 L w_2 - 28L^2 u_1\theta_2) \\ \frac{L}{840}(112L^2 u_2\theta_1 - 28L^2 u_2\theta_2 + 84Lu_2 w_1 - 84Lu_2 w_2 - 9w_2\theta_2^2 L^2 \\ -112L^2 u_1\theta_1 + 108\theta_1 L w_2^2 + 6\theta_1 L^3\theta_2^2 - 216w_1\theta_1 L w_2) \\ \frac{L}{30}(-3\theta_1 L w_2 - \theta_1 L^2\theta_2 + 18w_2^2 - 3w_2\theta_2 L + 2\theta_2^2 L^2) \\ \frac{1}{280}(-336Lu_2 w_1 + 336Lu_2 w_2 - 108w_2^2\theta_2 L + 36w_2\theta_2^2 L^2 \\ +28L^2 u_1\theta_1 - 108\theta_1 L w_2^2 - 3\theta_1 L^3\theta_2^2 + 216w_1\theta_1 L w_2 + 28L^2 u_1\theta_2) \\ \frac{L}{840}(-3\theta_1^3 L^3 - 216w_1 w_2\theta_2 L - 28L^2 u_2\theta_1 + 112L^2 u_2\theta_2 \\ +84Lu_2 w_1 - 84Lu_2 w_2 + 108w_2^2\theta_2 L + 9w_2\theta_2^2 L^2 + 28L^2 u_1\theta_1 - 9\theta_1 L^3\theta_2^2) \end{bmatrix}$$

$$+\frac{A}{L^3}\begin{bmatrix} 0 \\ \frac{1}{280}(108w_1^2\theta_1L+108w_1^2\theta_2L+36w_1\theta_2^2L^2+36w_1\theta_1^2L^2 \\ -36\theta_1^2L^2w_2+3\theta_1^3L^3\theta_2-336Lu_1w_1+336Lu_1w_2) \\ \frac{L}{840}(28L^2u_1\theta_2+108w_1^2\theta_1L+9w_1\theta_2^2L^2-9w_1\theta_1^2L^2 \\ +9\theta_1^2L^2w_2-9\theta_1^3L^3\theta_2-84Lu_1w_1+84Lu_1w_2) \\ 0 \\ \frac{1}{280}(-108w_1^2\theta_1L-108w_1^2\theta_2L-36w_1\theta_2^2L^2-36w_1\theta_1^2L^2 \\ +36\theta_1^2L^2w_2-3\theta_1^3L^3\theta_2+336Lu_1w_1-336Lu_1w_2) \\ \frac{L}{840}(-112L^2u_1\theta_2+108w_1^2\theta_2L-9w_1\theta_2^2L^2+9w_1\theta_1^2L^2 \\ -9\theta_1^2L^2w_2+6\theta_1^3L^3\theta_2-84Lu_1w_1+84Lu_1w_2) \end{bmatrix}$$

$$+B\begin{bmatrix} 0 \\ 0 \\ 1/2\theta_1^2 \\ 0 \\ 0 \\ -1/2\theta_2^2 \end{bmatrix}. \qquad (A.16)$$

Appendix B. Quadratic Jacobian of the reduced order model

Details of the quadratic Jacobian of Section 2.4 are specified here:

$$\boldsymbol{J}(t)=\begin{bmatrix} \boldsymbol{0} & \boldsymbol{I} \\ -\boldsymbol{K}_0 & -\boldsymbol{C}_0 \end{bmatrix}+\begin{bmatrix} \boldsymbol{0} & \boldsymbol{0} \\ -\boldsymbol{K}_c(t)-\boldsymbol{K}_L(t) & \boldsymbol{0} \end{bmatrix}+\begin{bmatrix} \boldsymbol{0} & \boldsymbol{0} \\ -\boldsymbol{K}_Q(t) & \boldsymbol{0} \end{bmatrix}, \qquad (B.1)$$

$$\boldsymbol{K}_0=\begin{bmatrix} \omega_1^2 & \cdots & 0 \\ \vdots & \ddots & \vdots \\ 0 & \cdots & \omega_L^2 \end{bmatrix}, \quad \boldsymbol{C}_0=2\begin{bmatrix} \xi_1\omega_1 & \cdots & 0 \\ \vdots & \ddots & \vdots \\ 0 & \cdots & \xi_L\omega_L \end{bmatrix},$$

$$\boldsymbol{K}_c(t)=\begin{bmatrix} \sum_{p=1}^{P}\Theta_{11}^{(p)}V_0^{(p)}X & \cdots & \sum_{p=1}^{P}\Theta_{1L}^{(p)}V_0^{(p)}X \\ \vdots & \ddots & \vdots \\ \sum_{p=1}^{P}\Theta_{L1}^{(p)}V_0^{(p)}X & \cdots & \sum_{p=1}^{P}\Theta_{LL}^{(p)}V_0^{(p)}X \end{bmatrix},$$

$$\boldsymbol{K}_L(t)=\begin{bmatrix} \sum_{k=1}^{L}B_{1k}^1q_k & \cdots & \sum_{k=1}^{L}B_{Lk}^1q_k \\ \vdots & \ddots & \vdots \\ \sum_{k=1}^{L}B_{1k}^Lq_k & \cdots & \sum_{k=1}^{L}B_{Lk}^Lq_k \end{bmatrix} \text{ with } \begin{cases} B_{jk}^i=\beta_{kj}^i & \text{if } j>k, \\ B_{jk}^i=\beta_{jk}^i & \text{if } j<k, \\ B_{jk}^i=2\beta_{jk}^i & \text{if } j=k, \end{cases}$$

$$\boldsymbol{K}_Q(t)=\begin{bmatrix} \sum_{k=1}^{L}\sum_{l\geq k}^{L}G_{1kl}^1q_kq_l & \cdots & \sum_{k=1}^{L}\sum_{l\geq k}^{L}G_{Lkl}^1q_kq_l \\ \vdots & \ddots & \vdots \\ \sum_{k=1}^{L}\sum_{l\geq k}^{L}G_{1kl}^Lq_kq_l & \cdots & \sum_{k=1}^{L}\sum_{l\geq k}^{L}G_{Lkl}^Lq_kq_l \end{bmatrix}$$

with

$$\begin{cases} G_{jkl}^i=3\Gamma_{jkl}^i & \text{if } j=k=l, \\ G_{jkk}^i=\Gamma_{jkk}^i & \text{if } j<k, \\ \quad=\Gamma_{kkj}^i & \text{if } j>k, \\ G_{jjk}^i=2\Gamma_{jjk}^i & \text{if } j<k, \\ \quad=2\Gamma_{kjj}^i & \text{if } j<k, \end{cases}$$

and

$$\begin{cases} G_{jkl}^i=\Gamma_{jkl}^i & \text{if } j<k<l, \\ \quad=\Gamma_{jlk}^i & \text{if } j<l<k, \\ \quad=\Gamma_{kjl}^i & \text{if } k<j<l, \\ \quad=\Gamma_{klj}^i & \text{if } k<l<j, \\ \quad=\Gamma_{lkj}^i & \text{if } l<k<j, \\ \quad=\Gamma_{ljk}^i & \text{if } l<j<k. \end{cases}$$

References

[1] K.L. Ekinci, M.L. Roukes, Nanoelectromechanical systems, Rev. Sci. Instrum. 76 (2005) 061101.

[2] K. Jensen, K. Kim, A. Zettl, An atomic resolution nanomechanical mass sensor, Nat. Nanotechnol. 3 (2008) 533–537.

[3] R. He, X.L. Feng, M.L. Roukes, P. Yang, Self-transducing silicon nanowire electromechanical systems at room temperature, Nano Lett. 8 (6) (2008) 1756–1761.

[4] I. Mahboob, H. Yamaguchi, Bit storage and bit flip operations in an electro-mechanical operator, Nat. Nanotechnol. 3 (2008) 275–279.

[5] V. Gouttenoire, T. Barois, S. Perisanu, J.-L. Leclercq, S.T. Purcell, P. Vincent, A. Ayari, Digital and FM demodulation of a doubly clamped single-walled carbon-nanotube oscillator: towards a nanotube cell phone, Small 6 (9) (2008) 1060–1065.

[6] N. Kacem, S. Hentz, D. Pinto, B. Reig, V. Nguyen, Nonlinear dynamics of nanomechanical beam resonators: improving the performance of NEMS-based sensors, Nanotechnology 20 (2009) 275501.

[7] A. Ayari, P. Vincent, S. Perisanu, M. Choueib, V. Gouttenoire, M. Bechelany, D. Cornu, S.T. Purcell, Self-oscillations in field emission nanowire mechanical resonators: a nanometric dc-ac conversion, Nano Lett. 7 (2007) 2252–2257.

[8] A. Lazarus, E. de Langre, P. Manneville, P. Vincent, S. Perisanu, A. Ayari, S.T. Purcell, Statics and dynamics of a nanowire in field emission, Int. J. Mech. Sci. 52 (2010) 1396–1406.

[9] R.B. Karabalin, M.H. Matheny, X.L. Feng, E. Defaÿ, G. Le Rhun, C. Marcoux, S. Hentz, P. Andreucci, M.L. Roukes, Piezoelectric nanoelectromechanical resonators based on aluminium nitride thin films, Appl. Phys. Lett. 95 (2009) 103111.

[10] E. Cattan, T. Haccart, G. Vélu, D. Rémiens, C. Bergaud, L. Nicu, Piezoelectric properties of PZT films for microcantilever, Sensors Actuators 74 (1999) 60–64.

[11] B. Cochelin, C. Vergez, A high order purely-based harmonic balance formulation for continuation of periodic solutions, J. Sound Vib. 324 (2009) 243–262.

[12] A. Lazarus, O. Thomas, A harmonic-based method for computing the stability of periodic solutions of dynamical systems, C. R. Méc. 338 (2010) 510–517.

[13] V. Kaajakari, T. Mattila, A. Oja, H. Seppä, Nonlinear limits for single-crystal silicon microresonators, J. Microelectromech. Syst. 13 (5) (2004) 715–724.

[14] S.C. Masmanidis, R.B. Karabalin, I. De Vlaminck, G. Borghs, M.R. Freeman, M.L. Roukes, Multifunctional nanomechanical systems via tunably coupled piezoelectric actuation, Science 317 (2007) 780–783.

[15] W. Szemplinska-Stupnicka, The Behavior of Nonlinear Vibrating Systems: Fundamental Concepts and Methods: Applications to Single-Degree-of-Freedom Systems, vol. 1, Kluwer Academic Publishers, 1990.

[16] A.H. Nayfeh, D.T. Mook, Nonlinear Oscillations, John Wiley & Sons, 1979.

[17] C. Touzé, O. Thomas, A. Chaigne, Asymmetric non-linear forced vibrations of free-edge circular plates, part 1: theory, J. Sound Vib. 258 (4) (2002) 649–676.

[18] O. Thomas, C. Touzé, A. Chaigne, Asymmetric non-linear forced vibrations of free-edge circular plates, part 2: experiments, J. Sound Vib. 265 (5) (2003) 1075–1101.

[19] O. Thomas, L. Nicu, C. Ayela, C. Touzé, Buckling and non-linear vibrations of a mems biosensor, in: ENOC-2008, Saint Petersburg, Russia, July 2008.

[20] H. Li, S. Preidikman, B. Balachandran, C.D. Mote Jr., Nonlinear free and forced oscillations of piezoelectric microresonators, J. Micromech. Microeng. 16 (2006) 356–367.

[21] M. Zamanian, S.E. Khadem, Nonlinear vibration of an electrically actuated microresonator tuned by combined DC piezoelectric and electric actuations, Smart Mater. Struct. 19 (2010) 015012.

[22] L. Azrar, S. Belouettar, J. Wauer, Nonlinear vibration analysis of actively loaded sandwich piezoelectric beams with geometric imperfections, Comput. Struct. 86 (2008) 2182–2191.

[23] S. Belouettar, L. Azrar, E.M. Daya, V. Laptev, M. Potier-Ferry, Active control of nonlinear vibration of sandwich piezoelectric beams: a simplified approach, Comput. Struct. 86 (2008) 386–397.

[24] S.N. Mahmoodi, M.F. Daqaq, N. Jalili, On the nonlinear-flexural response of piezoelectrically driven microcantilever sensors, Sensors Actuators A: Phys. 153 (2009) 171–179.

[25] S.N. Mahmoodi, N. Jalili, Non-linear vibrations and frequency response analysis of piezoelectrically driven microcantilevers, Int. J. Non-Linear Mech. 42 (2007) 577–587.

[26] M.-R. Ghazavi, G. Rezazadeh, S. Azizi, Pure parametric excitation of a micro cantilevers beam actuated by piezoelectric layers, Appl. Math. Modelling 34 (2010) 4196–4207.

[27] M.A. Crisfield, Non-Linear Finite Element Analysis of Solids and Structures, vol. 1, John Wiley & Sons, 1991.

[28] M.A. Crisfield, Non-Linear Finite Element Analysis of Solids and Structures, vol. 2, John Wiley & Sons, 1991.

[29] R. Lewandowski, Computational formulation for periodic vibration of geometrically nonlinear structures—part 1: theoretical background, Int. J. Solids Struct. 34 (15) (1997) 1925–1947.

[30] R. Lewandowski, Computational formulation for periodic vibration of geometrically nonlinear structures—part 1: numerical strategy and examples, Int. J. Solids Struct. 34 (15) (1997) 1949–1964.

[31] J.-X. Gao, Y.-P. Shen, Active control of geometrically nonlinear transient vibration of composite plates with piezoelectric actuators, J. Sound Vib. 264 (2003) 911–928.

[32] A. Mukherjee, A.S. Chaudhuri, Nonlinear dynamic response of piezolaminated smart beams, Comput. Struct. 83 (2005) 1298–1304.

[33] P. Apiwattanalunggarn, S.W. Shaw, P. Pierre, D. Jiang, Finite-element-based nonlinear modal reduction of a rotating beam with large-amplitude motion, J. Vib. Control 9 (3–4) (2003) 235–263.

[34] M. Peeters, R. Viguié, G. Sérandour, G. Kerschen, J.-C. Golinval, Nonlinear normal modes, part ii: toward a practical computation using numerical continuation techniques, Mech. Syst. Signal Process. 23 (2009) 195–216.

[35] M. Meyer, H.G. Matthies, Efficient model reduction in non-linear dynamics using the Karhunen–Loève expansion and dual-weighted-residual methods, Comput. Mech. 31 (2003) 179–191.

[36] Y.C. Liang, W.Z. Lin, H.P. Lee, S.P. Lim, K.H. Lee, H. Sun, Proper orthogonal decomposition and its applications—part II: model reduction for MEMS dynamical analysis, J. Sound Vib. 256 (2002) 515–532.

[37] M.I. McEwan, J.R. Wright, J.E. Cooper, A.Y.T. Leung, A combined modal/finite element analysis technique for the dynamic response of a non-linear beam to harmonic excitation, J. Sound Vib. 243 (4) (2001) 601–624.

[38] A.A. Muravyov, S.A. Rizzi, Determination of nonlinear stiffness with application to random vibration of geometrically nonlinear structures, Comput. Struct. 81 (2003) 1513–1523.

[39] M.P. Mignolet, C. Soize, Stochastics reduced order models for uncertain geometrically nonlinear dynamical systems, Comput. Methods Appl. Mech. Eng. 197 (2008) 3951–3963.

[40] P.M.A. Slaats, J. de Jongh, A.A.H.J. Sauren, Model reduction tools for nonlinear structural dynamics, Comput. Struct. 54 (1995) 1155–1171.

[41] P. Tiso, E. Jansen, M. Abdalla, A reduction method for finite element nonlinear dynamic analysis of shells, in: 47th Structures, Structural Dynamics and Material Conference, Newport, Rhode Island, May 2006, AIAA/ASME/ASCE/AHS/ASC.

[42] P. Tiso, D.J. Rixen, Reduction methods for MEMS nonlinear dynamic analysis, in: IMAC-XXVIII: International Modal Analysis Conference, Jacksonville, FL, February 2010.

[43] O. Thomas, J.-F. Deü, J. Ducarne, Vibrations of an elastic structure with shunted piezoelectric patches: efficient finite element formulation and electromechanical coupling coefficients, Int. J. Numer. Methods Eng. 80 (2009) 235–268.

[44] C. Maurini, J. Pouget, F. dell'Isola, Extension of the Euler–Bernoulli model of piezoelectric laminates to include 3D effects via a mixed approach, Comput. Struct. 4 (22–23) (2006) 1438–1458.

[45] R. Arquier, S. Karkar, A. Lazarus, O. Thomas, C. Vergez, B. Cochelin, Manlab: an interactive path-following and bifurcation analysis software ⟨http://manlab.lma.cnrs-mrs.fr/⟩.

[46] O. Thomas, A. Lazarus, C. Touzé, A harmonic-based method for computing the stability of periodic oscillations of nonlinear structural systems, in: Proceedings of the ASME 2010 IDETC/CIE 2010, Montreal, Quebec, Canada, August 2010.

[47] S. Guillon, D. Saya, L. Mazenq, S. Perisanu, P. Vincent, A. Lazarus, O. Thomas, L. Nicu, Effect of non-ideal clamping shape on the resonance frequencies of silicon nanocantilevers, Nanotechnology 22 (2011) 245501.

[48] M.A. Hopcroft, W.D. Nix, T.W. Kenny, What is the Young's modulus of silicon, J. Microelectromech. Syst. 19 (2) (2010) 229–238.

[49] R.B. Karabalin, S.C. Masmanidis, M.L. Roukes, Efficient parametric amplification in high and very high frequency piezoelectric nanoelectromechanical systems, Appl. Phys. Lett. 97 (2009) 183101.